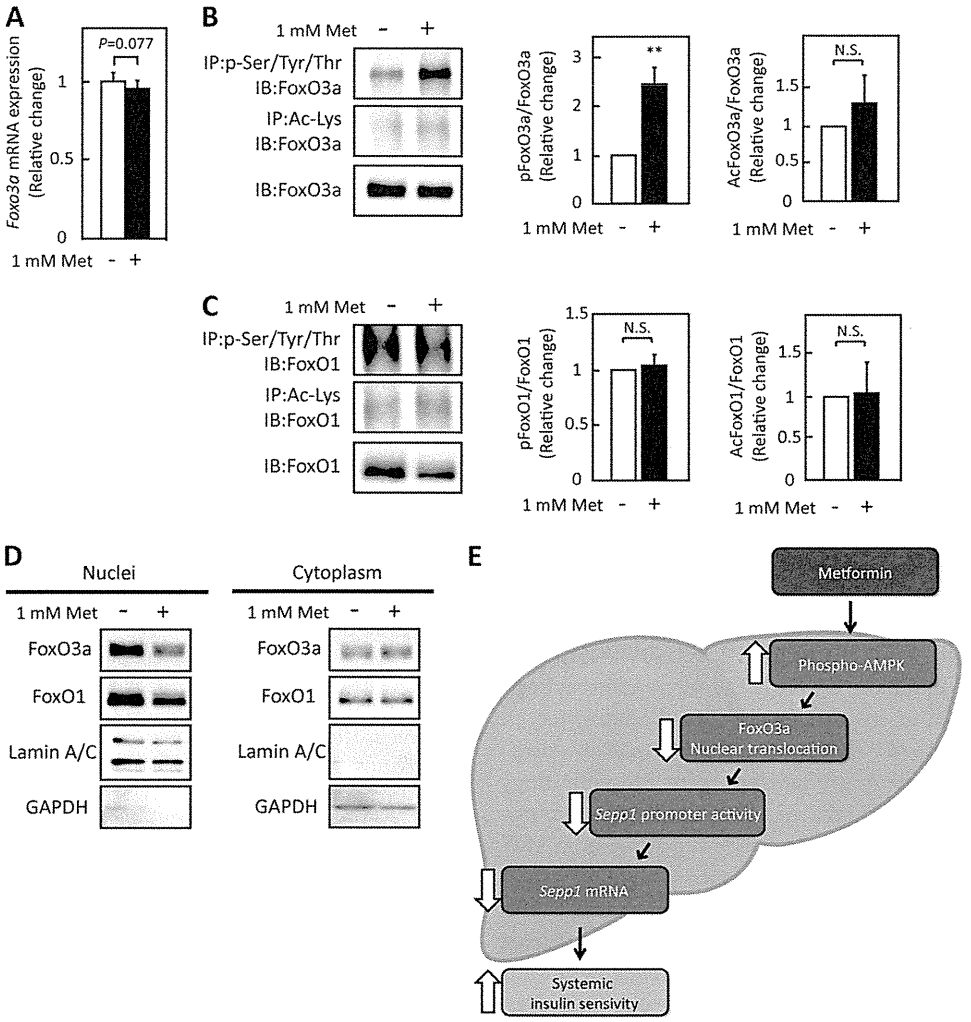

FIGURE 6. **Metformin treatment did not suppress FoxO3a expression but did suppress its activity.** *A*, *FoxO3a* mRNA expression in H4IIEC3 hepatocytes treated with metformin for 6 h. Expression values were normalized to *Actb* mRNA. Data represent means ± S.D. ($n = 5–6$). *B and C*, modification of FoxOs proteins by metformin treatment. Proteins were extracted after 6 h of metformin treatment. Immunoblotting was performed using anti-FoxO3a antibody (*B*) or anti-FoxO1 antibody (*C*). Data represent means ± S.D. ($n = 3$). **, $p < 0.01$. *N.S.*, not significant. *IP*, immunoprecipitation; *IB*, immunoblot. *D*, intracellular localization of FoxO3a and FoxO1 in H4IIEC3 hepatocytes upon treatment with metformin. Proteins were extracted after 6 h of metformin treatment. *E*, scheme of SeP suppression by metformin in the liver. FoxO3a positively regulates *SEPP1* promoter activity. Metformin suppresses FoxO3a activity via AMPK activation, resulting in suppression of SeP expression. Thus, the hypoglycemic effects of metformin may be mediated at least in part by SeP suppression in the liver.

FoxO3a participates in glucose homeostasis via regulation of the hepatic production of SeP, an insulin resistance-inducing hepatokine.

Knockdown of *Foxo3a*, but not *Foxo1*, rescued the cells from metformin-induced inactivation of the *SEPP1* promoter, although knockdown of both *Foxo3a* and *Foxo1* down-regulated *Sepp1* in the absence of metformin (Fig. 5, *A* and *B*). These results are in harmony with early reports showing that FoxO1 positively regulates *Sepp1* expression in cultured hepatocytes (38, 39). The current data suggest that both FoxO3a and FoxO1 positively regulate expression of *SEPP1* in the basal conditions, but FoxO3a has a dominant role in the suppression of *SEPP1* downstream of metformin/AMPK pathway in H4IIEC3 hepatocytes. Interestingly, metformin selectively phosphorylated and deacetylated FoxO3a but not FoxO1 (Fig. 6, *B* and *C*). This FoxO3a-selective phosphorylation by metformin is consistent with the previous report showing that AMPK-induced phosphorylation displays a strong preference toward FoxO3 compared with FoxO1 by using *in vitro* kinase assays (16).

The current study is the first to demonstrate the decreased nuclear localization and subsequent transcriptional inactivation of FoxO3a by AMPK downstream of metformin in the cultured hepatocytes. Greer *et al.* (16) identified FoxO3a as a direct phosphorylation target of AMPK using *in vitro* kinase assays. However, the authors reported that phosphorylation by AMPK increases FoxO3a transcriptional activity without affecting FOXO3A subcellular localization in mouse embryonic fibroblasts or 293T cells. A similar activation of FoxO3a by AMPK was reported in C2C12 myotubes (17). In this respect, our results suggest that the AMPK-induced inactivation of FoxO3a is hepatocyte-specific. When FoxO proteins are phosphorylated by Akt, the dissociation of nuclear co-factors from FoxO is thought to be required for nuclear exclusion of FoxO (40). Hence, the difference in nuclear co-activator/co-repressor

recruitment between hepatocytes and other cells might explain differences in the action of AMPK on FoxO3a cellular localization and transcriptional activity. Notably, the siRNA-induced knockdown of *Foxo3a* decreased *Sepp1* and *G6pc* mRNA levels in H4IIEC3 hepatocytes, suggesting that the AMPK/FoxO3a pathway in the liver regulates gluconeogenesis and the production of the hepatokine SeP. These findings shed light on a previously unrecognized role for the AMPK/FoxO3a pathway in the regulation of glucose metabolism in the liver.

The cancellation of the metformin-induced suppression of SeP by compound C, a known inhibitor of the AMPK pathway, was only partial (Fig. 2*B*). Likewise, the overexpression of FoxO3a only partially cancelled the suppressive action of metformin on *Sepp1* gene expression (Fig. 6, *D* and *E*). These results suggest that metformin decreases *Sepp1* gene expression through both AMPK/FoxO3a-dependent and other independent pathways. Recently, Kalender *et al.* (41) reported that metformin acts to suppress mTORC1 signaling in an AMPK-independent manner. In addition, Guigas *et al.* (42) found that metformin inhibits glucose phosphorylation in primary cultured hepatocytes independently of AMPK activity. Additional studies are needed to elucidate the AMPK-independent actions of metformin on *Sepp1* expression in H4IIEC3 hepatocytes.

The present sequence of *SEPP1* promoter completely corresponds to the refseq of the National Center for Biotechnology Information, but it misses one thymidine against the sequence of a previous report (21). This site had been reported as an SNP site (reference SNP ID rs201851607). Because both allele origin and minor allele frequency of this SNP site are not available, it is difficult to prove which genome sequence is "correct." At least this SNP site does not seem to affect basal *SEPP1* promoter activity. In addition, the metformin-responsible element identified in the current paper locates in the other region of the SNP site. Thus, we consider that the effect of this SNP on the conclusion of this paper is negligible.

A limitation of the present study is that the effects of metformin on SeP expression were not investigated in human samples. The metformin concentrations used in this study (0.25–1 mM) were higher than the blood levels of metformin in patients treated with conventional doses of the drug (10–40 μM). However, it has been pointed out that concentrations of metformin in liver tissue are much higher than those in the blood because the liver receives portal vein blood, which may contain materially higher doses of metformin than plasma (43). An early report indicated that metformin concentrations in the liver were greater than 250 μmol/kg in an STZ diabetic mouse model treated with 50 mg/kg metformin (44). One previous study used 0.25–1 mM metformin in rat primary hepatocytes as a more physiological range of intrahepatic concentration (43). In addition, we show that administration of 300 mg/kg metformin was effective on hepatic expression for *Sepp1* in C57BL/6J mice (Fig. 1*F*). Although clinical trials are necessary, we speculate here that treatment with metformin decreases blood levels of SeP in patients with diabetes. Additionally, the contribution of SeP suppression to the anti-diabetic actions of metformin should be confirmed by additional investigations using *Sepp1*-knock-out mice.

In summary, the present data provide a novel mechanism of action for metformin involving improvement of systemic insulin sensitivity via the regulation of SeP production (Fig. 6*E*) and suggest that AMPK/FoxO3a pathway in the liver may be a therapeutic target to the development of new anti-diabetic drugs.

Acknowledgments—We thank Dr. Atsushi Hirao (Kanazawa University) for providing a vector for FHRE-Luc and Maki Wakabayashi (Kanazawa University) for technical assistance. We thank Fabienne Foufelle (Université Pierre et Marie Curie) for providing adenovirus vector encoding DN-AMPK. We thank In-kyu Lee (Kyungpook National University) for providing adenovirus vector encoding CA-AMPK.

REFERENCES

1. Burk, R. F., and Hill, K. E. (2005) Selenoprotein P. An extracellular protein with unique physical characteristics and a role in selenium homeostasis. *Annu. Rev. Nutr.* **25,** 215–235
2. Carlson, B. A., Novoselov, S. V., Kumaraswamy, E., Lee, B. J., Anver, M. R., Gladyshev, V. N., and Hatfield, D. L. (2004) Specific excision of the selenocysteine tRNA[Ser]Sec (Trsp) gene in mouse liver demonstrates an essential role of selenoproteins in liver function. *J. Biol. Chem.* **279,** 8011–8017
3. Schomburg, L., Schweizer, U., Holtmann, B., Flohé, L., Sendtner, M., and Köhrle, J. (2003) Gene disruption discloses role of selenoprotein P in selenium delivery to target tissues. *Biochem. J.* **370,** 397–402
4. Hill, K. E., Zhou, J., McMahan, W. J., Motley, A. K., Atkins, J. F., Gesteland, R. F., and Burk, R. F. (2003) Deletion of selenoprotein P alters distribution of selenium in the mouse. *J. Biol. Chem.* **278,** 13640–13646
5. Misu, H., Takamura, T., Takayama, H., Hayashi, H., Matsuzawa-Nagata, N., Kurita, S., Ishikura, K., Ando, H., Takeshita, Y., Ota, T., Sakurai, M., Yamashita, T., Mizukoshi, E., Yamashita, T., Honda, M., Miyamoto, K., Kubota, T., Kubota, N., Kadowaki, T., Kim, H.-J., Lee, I., Minokoshi, Y., Saito, Y., Takahashi, K., Yamada, Y., Takakura, N., and Kaneko, S. (2010) A liver-derived secretory protein, selenoprotein P, causes insulin resistance. *Cell Metab.* **12,** 483–495
6. Wang, D.-S., Jonker, J. W., Kato, Y., Kusuhara, H., Schinkel, A. H., and Sugiyama, Y. (2002) Involvement of organic cation transporter 1 in hepatic and intestinal distribution of metformin. *J. Pharmacol. Exp. Ther.* **302,** 510–515
7. Shu, Y., Sheardown, S. A., Brown, C., Owen, R. P., Zhang, S., Castro, R. A., Ianculescu, A. G., Yue, L., Lo, J. C., Burchard, E. G., Brett, C. M., and Giacomini, K. M. (2007) Effect of genetic variation in the organic cation transporter 1 (OCT1) on metformin action. *J. Clin. Invest.* **117,** 1422–1431
8. Boyle, J. G., Salt, I. P., and McKay, G. A. (2010) Metformin action on AMP-activated protein kinase. A translational research approach to understanding a potential new therapeutic target. *Diabet. Med.* **27,** 1097–1106
9. Malin, S. K., Gerber, R., Chipkin, S. R., and Braun, B. (2012) Independent and combined effects of exercise training and metformin on insulin sensitivity in individuals with prediabetes. *Diabetes Care* **35,** 131–136
10. Singh, S., Akhtar, N., and Ahmad, J. (2012) Plasma adiponectin levels in women with polycystic ovary syndrome. Impact of Metformin treatment in a case-control study. *Diabetes Metab. Syndr.* **6,** 207–211
11. Shargorodsky, M., Omelchenko, E., Matas, Z., Boaz, M., and Gavish, D. (2012) Relation between augmentation index and adiponectin during one-year metformin treatment for nonalcoholic steatohepatosis. Effects beyond glucose lowering? *Cardiovasc. Diabetol.* **11,** 61
12. Medema, R. H., Kops, G. J., Bos, J. L., and Burgering, B. M. (2000) AFX-like Forkhead transcription factors mediate cell-cycle regulation by Ras and PKB through p27kip1. *Nature* **404,** 782–787
13. Luo, X., Puig, O., Hyun, J., Bohmann, D., and Jasper, H. (2007) Foxo and Fos regulate the decision between cell death and survival in response to UV irradiation. *EMBO J.* **26,** 380–390
14. Kops, G. J., Dansen, T. B., Polderman, P. E., Saarloos, I., Wirtz, K. W., Coffer, P. J., Huang, T.-T., Bos, J. L., Medema, R. H., and Burgering, B. M.

(2002) Forkhead transcription factor FOXO3a protects quiescent cells from oxidative stress. *Nature* **419,** 316–321
15. Olmos, Y., Valle, I., Borniquel, S., Tierrez, A., Soria, E., Lamas, S., and Monsalve, M. (2009) Mutual dependence of Foxo3a and PGC-1α in the induction of oxidative stress genes. *J. Biol. Chem.* **284,** 14476–14484
16. Greer, E. L., Oskoui, P. R., Banko, M. R., Maniar, J. M., Gygi, M. P., Gygi, S. P., and Brunet, A. (2007) The energy sensor AMP-activated protein kinase directly regulates the mammalian FOXO3 transcription factor. *J. Biol. Chem.* **282,** 30107–30119
17. Sanchez, A. M., Csibi, A., Raibon, A., Cornille, K., Gay, S., Bernardi, H., and Candau, R. (2012) AMPK promotes skeletal muscle autophagy through activation of forkhead FoxO3a and interaction with Ulk1. *J. Cell Biochem.* **113,** 695–710
18. Li, X.-N., Song, J., Zhang, L., LeMaire, S. A., Hou, X., Zhang, C., Coselli, J. S., Chen, L., Wang, X. L., Zhang, Y., and Shen, Y. H. (2009) Activation of the AMPK-FOXO3 pathway reduces fatty acid-induced increase in intracellular reactive oxygen species by upregulating thioredoxin. *Diabetes* **58,** 2246–2257
19. Lützner, N., Kalbacher, H., Krones-Herzig, A., and Rösl, F. (2012) FOXO3 is a glucocorticoid receptor target and regulates LKB1 and its own expression based on cellular AMP levels via a positive autoregulatory loop. *PLoS One* **7,** e42166
20. Honda, M., Takehana, K., Sakai, A., Tagata, Y., Shirasaki, T., Nishitani, S., Muramatsu, T., Yamashita, T., Nakamoto, Y., Mizukoshi, E., Sakai, Y., Yamashita, T., Nakamura, M., Shimakami, T., Yi, M., Lemon, S. M., Suzuki, T., Wakita, T., and Kaneko, S. (2011) Malnutrition impairs interferon signaling through mTOR and FoxO pathways in patients with chronic hepatitis C. *Gastroenterology* **141,** 128–140, 140.e1–140.e2
21. Dreher, I., Jakobs, T. C., and Köhrle, J. (1997) Cloning and characterization of the human selenoprotein P promoter. Response of selenoprotein P expression to cytokines in liver cells. *J. Biol. Chem.* **272,** 29364–29371
22. Takebe, G., Yarimizu, J., Saito, Y., Hayashi, T., Nakamura, H., Yodoi, J., Nagasawa, S., and Takahashi, K. (2002) A comparative study on the hydroperoxide and thiol specificity of the glutathione peroxidase family and selenoprotein P. *J. Biol. Chem.* **277,** 41254–41258
23. Nakamura, S., Takamura, T., Matsuzawa-Nagata, N., Takayama, H., Misu, H., Noda, H., Nabemoto, S., Kurita, S., Ota, T., Ando, H., Miyamoto, K., and Kaneko, S. (2009) Palmitate induces insulin resistance in H4IIEC3 hepatocytes through reactive oxygen species produced by mitochondria. *J. Biol. Chem.* **284,** 14809–14818
24. Flicek, P., Amode, M. R., Barrell, D., Beal, K., Brent, S., Carvalho-Silva, D., Clapham, P., Coates, G., Fairley, S., Fitzgerald, S., Gil, L., Gordon, L., Hendrix, M., Hourlier, T., Johnson, N., Kähäri, A. K., Keefe, D., Keenan, S., Kinsella, R., Komorowska, M., Koscielny, G., Kulesha, E., Larsson, P., Longden, I., McLaren, W., Muffato, M., Overduin, B., Pignatelli, M., Pritchard, B., Riat, H. S., Ritchie, G. R., Ruffier, M., Schuster, M., Sobral, D., Tang, Y. A., Taylor, K., Trevanion, S., Vandrovcova, J., White, S., Wilson, M., Wilder, S. P., Aken, B. L., Birney, E., Cunningham, F., Dunham, I., Durbin, R., Fernández-Suarez, X. M., Harrow, J., Herrero, J., Hubbard, T. J., Parker, A., Proctor, G., Spudich, G., Vogel, J., Yates, A., Zadissa, A., and Searle, S. M. (2012) Ensembl 2012. *Nucleic Acids Res.* **40,** D84–D90
25. Paten, B., Herrero, J., Beal, K., Fitzgerald, S., and Birney, E. (2008) Enredo and Pecan. Genome-wide mammalian consistency-based multiple alignment with paralogs. *Genome Res.* **18,** 1814–1828
26. Wingender, E. (2008) The TRANSFAC project as an example of framework technology that supports the analysis of genomic regulation. *Brief. Bioinform.* **9,** 326–332
27. Kel, A. E., Gössling, E., Reuter, I., Cheremushkin, E., Kel-Margoulis, O. V., and Wingender, E. (2003) MATCH. A tool for searching transcription factor binding sites in DNA sequences. *Nucleic Acids Res.* **31,** 3576–3579
28. Speckmann, B., Sies, H., and Steinbrenner, H. (2009) Attenuation of hepatic expression and secretion of selenoprotein P by metformin. *Biochem. Biophys. Res. Commun.* **387,** 158–163
29. Łukaszewicz-Hussain, A., and Moniuszko-Jakoniuk, J. (2004) Liver catalase, glutathione peroxidase, and reductase activity, reduced glutathione and hydrogen peroxide levels in acute intoxication with chlorfenvinphos, an organophosphate insecticide. *Pol. J. Environ. Stud.* **13,** 303–309
30. Magwere, T., Naik, Y. S., and Hasler, J. A. (1997) Effects of chloroquine treatment on antioxidant enzymes in rat liver and kidney. *Free Radic. Biol. Med.* **22,** 321–327
31. Zhou, G., Myers, R., Li, Y., Chen, Y., Shen, X., Fenyk-Melody, J., Wu, M., Ventre, J., Doebber, T., Fujii, N., Musi, N., Hirshman, M. F., Goodyear, L. J., and Moller, D. E. (2001) Role of AMP-activated protein kinase in mechanism of metformin action. *J. Clin. Invest.* **108,** 1167–1174
32. Brunet, A., Bonni, A., Zigmond, M. J., Lin, M. Z., Juo, P., Hu, L. S., Anderson, M. J., Arden, K. C., Blenis, J., and Greenberg, M. E. (1999) Akt promotes cell survival by phosphorylating and inhibiting a Forkhead transcription factor. *Cell* **96,** 857–868
33. Eckers, A., Sauerbier, E., Anwar-Mohamed, A., Hamann, I., Esser, C., Schroeder, P., El-Kadi, A. O., and Klotz, L.-O. (2011) Detection of a functional xenobiotic response element in a widely employed FoxO-responsive reporter construct. *Arch. Biochem. Biophys.* **516,** 138–145
34. Cantó, C., Gerhart-Hines, Z., Feige, J. N., Lagouge, M., Noriega, L., Milne, J. C., Elliott, P. J., Puigserver, P., and Auwerx, J. (2009) AMPK regulates energy expenditure by modulating NAD^+ metabolism and SIRT1 activity. *Nature* **458,** 1056–1060
35. Puigserver, P., Rhee, J., Donovan, J., Walkey, C. J., Yoon, J. C., Oriente, F., Kitamura, Y., Altomonte, J., Dong, H., Accili, D., and Spiegelman, B. M. (2003) Insulin-regulated hepatic gluconeogenesis through FOXO1-PGC-1α interaction. *Nature* **423,** 550–555
36. Hosaka, T., Biggs, W. H., 3rd, Tieu, D., Boyer, A. D., Varki, N. M., Cavenee, W. K., and Arden, K. C. (2004) Disruption of forkhead transcription factor (FOXO) family members in mice reveals their functional diversification. *Proc. Natl. Acad. Sci. U.S.A.* **101,** 2975–2980
37. Haeusler, R. A., Kaestner, K. H., and Accili, D. (2010) FoxOs function synergistically to promote glucose production. *J. Biol. Chem.* **285,** 35245–35248
38. Speckmann, B., Walter, P. L., Alili, L., Reinehr, R., Sies, H., Klotz, L.-O., and Steinbrenner, H. (2008) Selenoprotein P expression is controlled through interaction of the coactivator PGC-1α with FoxO1a and hepatocyte nuclear factor 4α transcription factors. *Hepatology* **48,** 1998–2006
39. Walter, P. L., Steinbrenner, H., Barthel, A., and Klotz, L.-O. (2008) Stimulation of selenoprotein P promoter activity in hepatoma cells by FoxO1a transcription factor. *Biochem. Biophys. Res. Commun.* **365,** 316–321
40. Van Der Heide, L. P., Hoekman, M. F., and Smidt, M. P. (2004) The ins and outs of FoxO shuttling. Mechanisms of FoxO translocation and transcriptional regulation. *Biochem. J.* **380,** 297–309
41. Kalender, A., Selvaraj, A., Kim, S. Y., Gulati, P., Brûlé, S., Viollet, B., Kemp, B. E., Bardeesy, N., Dennis, P., Schlager, J. J., Marette, A., Kozma, S. C., and Thomas, G. (2010) Metformin, independent of AMPK, inhibits mTORC1 in a rag GTPase-dependent manner. *Cell Metab.* **11,** 390–401
42. Guigas, B., Bertrand, L., Taleux, N., Foretz, M., Wiernsperger, N., Vertommen, D., Andreelli, F., Viollet, B., and Hue, L. (2006) 5-Aminoimidazole-4-carboxamide-1-β-D-ribofuranoside and metformin inhibit hepatic glucose phosphorylation by an AMP-activated protein kinase-independent effect on glucokinase translocation. *Diabetes* **55,** 865–874
43. Foretz, M., Hébrard, S., Leclerc, J., Zarrinpashneh, E., Soty, M., Mithieux, G., Sakamoto, K., Andreelli, F., and Viollet, B. (2010) Metformin inhibits hepatic gluconeogenesis in mice independently of the LKB1/AMPK pathway via a decrease in hepatic energy state. *J. Clin. Invest.* **120,** 2355–2369
44. Wilcock, C., and Bailey, C. J. (1994) Accumulation of metformin by tissues of the normal and diabetic mouse. *Xenobiotica* **24,** 49–57

Research Article

EASL EUROPEAN ASSOCIATION FOR THE STUDY OF THE LIVER | JOURNAL OF HEPATOLOGY

The transcription factor SALL4 regulates stemness of EpCAM-positive hepatocellular carcinoma

Sha Sha Zeng[1], Taro Yamashita[1,2,*], Mitsumasa Kondo[1], Kouki Nio[1], Takehiro Hayashi[1], Yasumasa Hara[1], Yoshimoto Nomura[1], Mariko Yoshida[1], Tomoyuki Hayashi[1], Naoki Oishi[1], Hiroko Ikeda[3], Masao Honda[1], Shuichi Kaneko[1]

[1]*Department of Gastroenterology, Kanazawa University Hospital, Kanazawa, Ishikawa, Japan;* [2]*Department of General Medicine, Kanazawa University Hospital, Kanazawa, Ishikawa, Japan;* [3]*Department of Pathology, Kanazawa University Hospital, Kanazawa, Ishikawa, Japan*

Background & Aims: Recent evidence suggests that hepatocellular carcinoma can be classified into certain molecular subtypes with distinct prognoses based on the stem/maturational status of the tumor. We investigated the transcription program deregulated in hepatocellular carcinomas with stem cell features.

Methods: Gene and protein expression profiles were obtained from 238 (analyzed by microarray), 144 (analyzed by immunohistochemistry), and 61 (analyzed by qRT-PCR) hepatocellular carcinoma cases. Activation/suppression of an identified transcription factor was used to evaluate its role in cell lines. The relationship of the transcription factor and prognosis was statistically examined.

Results: The transcription factor SALL4, known to regulate stemness in embryonic and hematopoietic stem cells, was found to be activated in a hepatocellular carcinoma subtype with stem cell features. SALL4-positive hepatocellular carcinoma patients were associated with high values of serum alpha fetoprotein, high frequency of hepatitis B virus infection, and poor prognosis after surgery compared with SALL4-negative patients. Activation of SALL4 enhanced spheroid formation and invasion capacities, key characteristics of cancer stem cells, and up-regulated the hepatic stem cell markers *KRT19*, *EPCAM*, and *CD44* in cell lines. Knockdown of SALL4 resulted in the down-regulation of these stem cell markers, together with attenuation of the invasion capacity. The SALL4 expression status was associated with histone deacetylase activity in cell lines, and the histone deacetylase inhibitor successfully suppressed proliferation of SALL4-positive hepatocellular carcinoma cells.

Conclusions: SALL4 is a valuable biomarker and therapeutic target for the diagnosis and treatment of hepatocellular carcinoma with stem cell features.

Keywords: Cancer stem cell; Hepatocellular carcinoma; Gene expression profile; Chemosensitivity.

Received 15 March 2013; received in revised form 27 August 2013; accepted 28 August 2013; available online 6 September 2013

* Corresponding author. Address: Department of General Medicine/Gastroenterology, Kanazawa University Hospital, 13-1 Takara-Machi, Kanazawa, Ishikawa 920-8641, Japan. Tel.: +81 76 265 2042; fax: +81 76 234 4281.

E-mail address: taroy@m-kanazawa.jp (T. Yamashita).

Abbreviations: CSC, cancer stem cell; HCC, hepatocellular carcinoma; EpCAM, epithelial cell adhesion molecule; AFP, alpha fetoprotein; HpSC-HCC, hepatic stem cell-like HCC; MH-HCC, mature hepatocyte-like HCC; SALL4, Sal-like 4 (Drosophila); qRT-PCR, quantitative reverse transcription-polymerase chain reaction; HDAC, histone deacetylase; SAHA, suberoylanilide hydroxamic acid; SBHA, suberic bis-hydroxamic acid; NuRD, nucleosome remodeling and deacetylase.

Introduction

Cancer is a heterogeneous disease in terms of morphology and clinical behavior. This heterogeneity has traditionally been explained by the clonal evolution of cancer cells and the accumulation of serial stochastic genetic/epigenetic changes [1]. The alteration of the microenvironment by tumor stromal cells is also considered to contribute to the development of the heterogeneous nature of the tumor through the activation of various signaling pathways in cancer cells, including epithelial mesenchymal transition programs [2].

Recent evidence suggests that a subset of tumor cells with stem cell features, known as cancer stem cells (CSCs), are capable of self-renewal and can give rise to relatively differentiated cells, thereby forming heterogeneous tumor cell populations [3]. CSCs were also found to generate tumors more efficiently in immunodeficient mice than non-cancer stem cells in various solid tumors as well as hematological malignancies [4]. CSCs are also more metastatic and chemo/radiation-resistant than non-CSCs and are therefore considered to be a pivotal target for tumor eradication [5,6].

Hepatocellular carcinoma (HCC) is a leading cause of cancer death worldwide [7]. Recently, we proposed a novel HCC classification system based on the expression status of the hepatic stem/progenitor markers epithelial cell adhesion molecule (EpCAM) and alpha fetoprotein (AFP) [8]. EpCAM-positive ($^+$) AFP$^+$ HCC (hepatic stem cell-like HCC; HpSC-HCC) is characterized by an onset of disease at younger ages, activation of Wnt/β-catenin signaling, a high frequency of portal vein invasion and poor

prognosis after radical resection, compared with EpCAM$^-$ AFP$^-$ HCC (mature hepatocyte-like HCC; MH-HCC) [9]. *EPCAM* is a target gene of Wnt/β-catenin signaling, and EpCAM$^+$ HCC cells isolated from primary HCC and cell lines show CSC features including tumorigenicity, invasiveness, and resistance to fluorouracil [9,10]. Thus, EpCAM appears to be a potentially useful marker for the isolation of liver CSCs in HpSC-HCC. However, key transcriptional programs responsible for the maintenance of EpCAM$^+$ CSCs are still unclear.

In this study, we aimed to clarify the transcriptional programs deregulated in HpSC-HCC using a gene expression profiling approach. We found that the *SALL4* gene encoding Sal-like 4 (*Drosophila*) (SALL4), a zinc finger transcriptional activator and vertebrate orthologue of the *Drosophila* gene spalt (*sal*) [11], was up-regulated in HpSC-HCC. In adults, *SALL4* is known to be expressed in hematopoietic stem cells and their malignancies, but its role in HCC has not yet been fully elucidated [12–14]. We therefore investigated the role of SALL4 in the regulation and maintenance of EpCAM$^+$ HCC.

Materials and methods

Clinical HCC specimens

A total of 144 HCC tissues and adjacent non-cancerous liver tissues were obtained from patients who underwent hepatectomy for HCC treatment from 2002 to 2010 at Kanazawa University Hospital, Kanazawa, Japan. These samples were formalin-fixed and paraffin-embedded, and used for immunohistochemistry (IHC). A further 61 HCC samples were obtained from patients who underwent hepatectomy from 2008 to 2011; these were freshly snap-frozen in liquid nitrogen and used for RNA analysis. Of these 61 HCCs, 8 and 36 cases were defined as HpSC-HCC and MH-HCC, respectively, according to previously described criteria [8].

27 HCC cases were included in both the IHC cohort (n = 144) and quantitative reverse transcription-polymerase chain reaction (qRT-PCR) cohort (n = 61), and SALL4 gene and protein expression were compared between these cases. An additional fresh HpSC-HCC sample was obtained from a surgically resected specimen and immediately used for preparation of a single-cell suspension. All experimental and tissue acquisition procedures were approved by the Ethics Committee and the Institutional Review Board of Kanazawa University Hospital. All patients provided written informed consent.

Microarray analysis

Detailed information on microarray analysis is available in the Supplementary Materials and methods.

Cell culture and reagents

Human liver cancer cell lines HuH1, HuH7, HLE, and HLF were obtained from the Japanese Collection of Research Bioresources (JCRB), and Hep3B and SK-Hep-1 were obtained from the American Type Culture Collection (ATCC). Single-cell suspensions of primary HCC tissue were prepared as described previously [15]. Detailed information is available in the Supplementary Materials and methods. The histone deacetylase (HDAC) inhibitor suberic bis-hydroxamic acid (SBHA) and suberoylanilide hydroxamic acid (SAHA) were obtained from Cayman Chemical (Ann Arbor, MI). Plasmid constructs pCMV6-SALL4 (encoding *SALL4A*), pCMV6-SALL4-GFP, and 29mer shRNA constructs against human SALL4 (No. 7412) were obtained from OriGene Technologies, Inc. (Rockville, MD). These constructs were transfected using Lipofectamine 2000 (Life Technologies, Carlsbad, CA) according to the manufacturer's protocol.

Western blotting

Whole cell lysates were prepared using RIPA lysis buffer. Nuclear and cytoplasmic proteins were extracted using NE-PER Nuclear and Cytoplasmic Extraction Reagents (Pierce Biotechnology Inc., Rockford, IL). Mouse monoclonal antibody to human Sall4 clone 6E3 (Abnova, Walnut, CA), rabbit polyclonal antibodies to human Lamin B1 (Cell Signaling Technology Inc., Danvers, MA), and mouse monoclonal anti-β-actin antibody (Sigma-Aldrich, St. Louis, MO) were used. Immune complexes were visualized by enhanced chemiluminescence (Amersham Biosciences Corp., Piscataway, NJ) as described previously [15,16].

Quantitative reverse transcription-polymerase chain reaction (qRT-PCR)

Detailed information on qRT-PCR is available in the Supplementary Materials and methods.

IHC and immunofluorescence (IF) analyses

IHC was performed using an Envision+ kit (Dako, Carpinteria, CA) according to the manufacturer's instructions. Anti-SALL4 monoclonal antibody 6E3 (Abnova, Walnut, CA), anti-EpCAM monoclonal antibody VU-1D9 (Oncogene Research Products, San Diego, CA), and anti-CK19 monoclonal antibody RCK108 (Dako Japan, Tokyo, Japan) were used for detecting SALL4, EpCAM, and CK19, respectively. Anti-Sall4 rabbit polyclonal antibodies (ab29112) (Abnova) and vector red (Vector Laboratories Inc., Burlingame, CA) were used for double color IHC analysis. Samples with >5% positive staining in a given area were considered to be positive for a particular antibody. For IF analyses, Alexa 488 fluorescein isothiocyanate (FITC)-conjugated anti-mouse immunoglobulin G (IgG) (Life Technologies) was used as a secondary antibody.

Cell proliferation, spheroid formation, invasion, and HDAC activity assay

Detailed information on this topic is available in the Supplementary Materials and methods.

Statistical analyses

Student's *t* tests were performed with GraphPad Prism software 5.0 (GraphPad Software, San Diego, CA) to compare various test groups assayed by cell proliferation assays and qRT-PCR analysis. Spearman's correlation analysis and Kaplan-Meier survival analysis were also performed with GraphPad Prism software 5.0 (GraphPad Software).

Results

Activation of SALL4 in HpSC-HCC

To elucidate the transcriptional programs deregulated in HpSC-HCC, we performed class-comparison analyses and identified 793 genes showing significant differences in differential expression between HpSC-HCC (n = 60) and MH-HCC (n = 96) (p <0.001), as previously described [9]. Of them, 455 genes were specifically up-regulated in HpSC-HCC, and we performed transcription factor analysis using this gene set to identify their transcriptional regulators by MetaCore software. We identified four transcription factor genes, *SALL4*, *NFYA*, *TP53*, and *SP1*, that were potentially activated in HpSC-HCC (Fig. 1A). Involvement of *TP53* and *SP1* in the stemness of HCC has previously been described [17,18], but the roles of *SALL4* and *NFYA* were unclear.

We investigated the interaction networks affected by *SALL4* and *NFYA* using the MetaCore dataset. We showed that *SALL4* might be a regulator of Akt signaling (*SP1*), Wnt signaling (*TCF7L2*), and epigenetic modification (*JARID2*, *DMRT1*, *DNMT3B*) [19], and could potentially regulate two other transcriptional regulators, *SP1* and *NFYA*, through Akt and Myb signaling pathways (Fig. 1B). As a recent study indicated that *SALL4* is a direct target of the Wnt signaling pathway [20], which is dominantly activated in HpSC-HCC [9], we focused on the expression of *SALL4* in HpSC-HCC, and confirmed its up-regulation in HpSC-HCC compared

A

Transcription factors	*p* value	z-score
SALL4	0.0005708	3.958
NFYA	0.002483	3.267
TP53	3.923E-05	4.25
SP1	2.917E-11	6.942

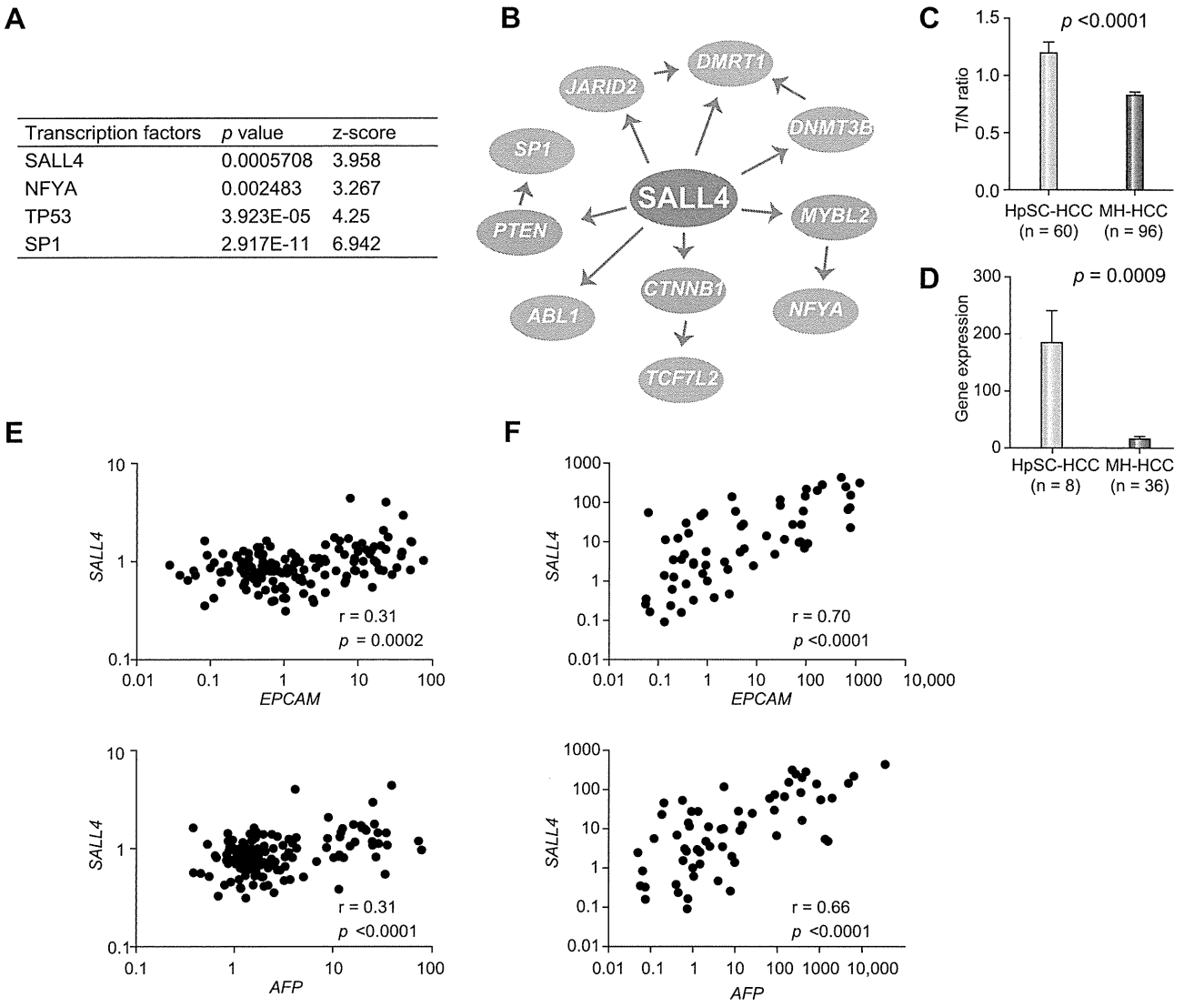

Fig. 1. Transcription factors potentially activated in HpSC-HCC. (A) Transcription factor analysis. Transcription factors regulating genes up-regulated in HpSC-HCC are listed with their *p* values and z-scores as calculated by MetaCore software. (B) Interaction network analysis. Seven genes (*ABL1*, *DMRT1*, *DNMT3B*, *JARID2*, *NFYA*, *SP1*, and *TCF7L2*, indicated in orange) shown to be up-regulated in HpSC-HCC were identified as potential target genes regulated by *SALL4* (indicated in red). (C) *SALL4* gene expression evaluated by microarray analysis. Tumor/non-tumor (T/N) ratios of microarray data in HpSC-HCC (n = 60) and MH-HCC (n = 96). (D) *SALL4* gene expression evaluated by qRT-PCR. Gene expression of *SALL4* in HpSC-HCC (n = 8) and MH-HCC (n = 36) samples. (E) Scatter plot analysis. Gene expression levels of *EPCAM* (upper panel) and *AFP* (lower panel) were positively correlated with those of *SALL4* in microarray data (n = 238, T/N ratios), as shown by Spearman's correlation coefficients. (F) Scatter plot analysis. Gene expression levels of *EPCAM* (upper panel) and *AFP* (lower panel) were positively correlated with those of *SALL4* in qRT-PCR data (n = 61), as shown by Spearman's correlation coefficients. (This figure appears in colour on the web.)

with MH-HCC as evaluated by microarray data (Fig. 1C). We validated this using an independent HCC cohort evaluated by qRT-PCR (Fig. 1D). We further examined the expression of *SALL4*, *EPCAM*, and *AFP* using microarray data of 238 HCC cases (Fig. 1E) and qRT-PCR data of 61 HCC cases (Fig. 1F). For the tumor/non-tumor ratios, we identified a weak positive correlation between *SALL4* and *EPCAM* ($r = 0.31$, $p < 0.0001$) and between *SALL4* and *AFP* ($r = 0.31$, $p = 0.0003$) in the microarray cohort. We further evaluated expression of these genes in HCC tissues by qRT-PCR, and we validated the strong positive correlation between *SALL4* and *EPCAM* ($r = 0.70$, $p < 0.0001$) and between *SALL4* and AFP ($r = 0.66$, $p < 0.0001$) in the independent cohort.

Next we performed IHC analysis of 144 HCC cases surgically resected at Kanazawa University Hospital. We first confirmed the nuclear accumulation of SALL4 stained by an anti-human SALL4 antibody (Fig. 2A). We further confirmed the concordance of SALL4 protein expression evaluated by IHC, and *SALL4* gene expression evaluated by qRT-PCR using the same samples (Fig. 2B). We detected the nuclear expression of SALL4 in 43 of 144 HCC cases (Table 1). After evaluating the clinicopathological characteristics of SALL4-positive and -negative HCC cases, we identified that SALL4-positive HCCs were associated with a significantly high frequency of hepatitis B virus (HBV) infection and significantly high serum AFP values. We further identified that

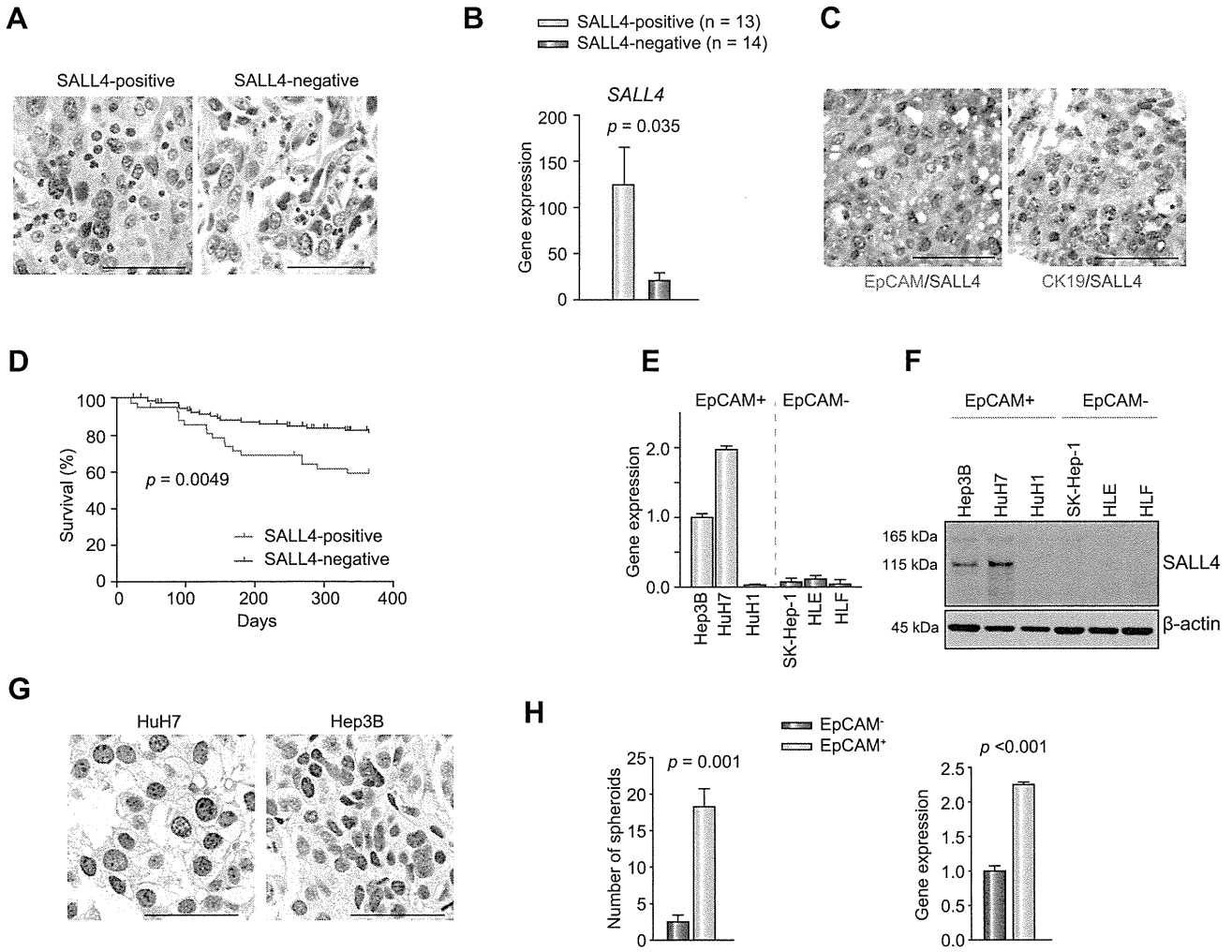

Fig. 2. SALL4 expression in human primary HCCs and cell lines. (A) Representative images of SALL4-positive and -negative HCC immunostaining (scale bar, 100 μm). (B) Gene expression of *SALL4* in SALL4-positive (n = 13) and -negative HCCs (n = 14) as shown by IHC (mean ± SD). (C) Double color IHC analysis of HCC stained with anti-SALL4 and anti-EpCAM or anti-CK19 antibodies (scale bar, 100 μm). (D) Kaplan-Meier survival analysis with Log-rank. Recurrence-free survival of SALL4-positive (n = 43) and -negative (n = 101) HCCs was analyzed. (E) *SALL4* expression in EpCAM$^+$ (Hep3B, HuH7, and HuH1) and EpCAM$^-$ (SK-Hep-1, HLE, and HLF) HCC cell lines evaluated by qRT-PCR. (F) SALL4 expression in EpCAM$^+$ and EpCAM$^-$ HCC cell lines evaluated by Western blotting. (G) IHC analysis of SALL4 expression in subcutaneous tumors obtained from EpCAM$^+$ (HuH7 and Hep3B) HCC cell lines xenografted in NOD/SCID mice. (H) Spheroid formation capacity of sorted EpCAM$^+$ and EpCAM$^-$ cells obtained from a primary HCC. Number of spheroids obtained from 2000 sorted cells is indicated (n = 3, mean ± SD). Gene expression of *SALL4* in sorted EpCAM$^+$ and EpCAM$^-$ cells obtained from a primary HCC (n = 3, mean ± SD). (This figure appears in colour on the web.)

SALL4-positive HCCs were associated with expression of the hepatic stem cell markers EpCAM and CK19. Co-expression of SALL4, EpCAM, and CK19 was confirmed by double color IHC analysis (Fig. 2C). Evaluation of the survival outcome of these surgically resected HCC cases by Kaplan-Meier survival analysis indicated that SALL4-positive HCCs were associated with significantly lower recurrence-free survival outcomes within one year compared with SALL4-negative HCCs ($p = 0.0049$) (Fig. 2D).

Because SALL4 expression was positively correlated with EpCAM and AFP expression in primary HCC cases, we evaluated the expression of SALL4 in EpCAM$^+$ AFP$^+$ and EpCAM$^-$ AFP$^-$ HCC cell lines. Consistent with the primary HCC data, two of three EpCAM$^+$ AFP$^+$ HCC cell lines (Hep3B and HuH7) abundantly expressed SALL4, as shown by qRT-PCR (Fig. 2E) and Western blotting (Fig. 2F). We identified the expression of two isoforms of SALL4 proteins with molecular weights of 165 kDa (SALL4A) and 115 kDa (SALL4B), and SALL4B was found to be the dominant endogenous isoform in HCC cell lines. All EpCAM$^-$ AFP$^-$ HCC cell lines (SK-Hep-1, HLE, and HLF) and one EpCAM$^+$ AFP$^+$ cell line (HuH1) did not express SALL4. Nuclear accumulation of SALL4 in Hep3B and HuH7 cells was confirmed by IHC using subcutaneous tumors developed in xenotransplanted NOD/SCID mice (Fig. 2G). We further evaluated the expression of *EPCAM* and *SALL4* using single cell suspensions derived from a surgically resected primary HCC. EpCAM$^+$ and EpCAM$^-$ cells were separated by magnetic beads, and we revealed a strong spheroid formation capacity of sorted EpCAM$^+$ cells compared with EpCAM$^-$ cells (Fig. 2H, left panel). Interestingly, when comparing the expression of *SALL4* in these sorted cells, we identified a high expression of *SALL4* in sorted EpCAM$^+$ cells compared with EpCAM$^-$ cells (Fig. 2H, right panel), indicating that SALL4 is activated in EpCAM$^+$ liver CSCs.

Table 1. Clinicopathological characteristics of SALL4-positive and -negative HCC cases used for IHC analyses.

Parameters	SALL4-positive (n = 43)	SALL4-negative (n = 101)	*p* value*
Age (yr, mean ± SE)	60.8 ± 1.8	64.6 ± 1.0	0.13
Sex (male/female)	27/16	70/18	0.06
Etiology (HBV/HCV/B + C/other)	21/14/0/8	20/63/3/15	0.0014
Liver cirrhosis (yes/no)	21/22	61/40	0.27
AFP (ng/ml, mean ± SE)	13,701 ± 9292	175.5 ± 55.0	<0.0001
Histological grade**			
I-II	3	18	
II-III	33	68	
III-IV	7	15	0.24
Tumor size (<3 cm/>3 cm)	17/26	57/44	0.071
EpCAM (positive/negative)	27/16	29/72	0.0002
CK19 (positive/negative)	12/31	12/89	0.027

*Mann-Whitney U-test or χ^2 test.
**Edmondson-Steiner.

SALL4 regulates stemness of HpSC-HCC

To explore the role of SALL4 in HpSC-HCC, we evaluated the effect of its overexpression in HuH1 cells which showed little expression of SALL4 irrespective of EpCAM$^+$ and AFP$^+$ HpSC-HCC phenotype. We transfected plasmid constructs encoding SALL4 (pCMV6-SALL4) or control (pCMV7), and we similarly identified the expression of two isoforms by using this construct (Fig. 3A). Evaluation of the subcellular localization of GFP-tagged SALL4 (pCMV6-SALL4-GFP) showed that it could be detected in both the cytoplasm and nucleus (Fig. 3B). We observed strong up-regulation of the hepatic stem cell marker *KRT19*, modest up-regulation of *EPCAM* and *CD44*, and down-regulation of the mature hepatocyte marker *ALB* in HuH1 cells transfected with pCMV6-SALL4 compared with the control (Fig. 3C). Up-regulation of CK19 by SALL4 overexpression was also confirmed at the protein level by IF analysis (Fig. 3D). Phenotypically, SALL4 overexpression in HuH1 cells resulted in the significant activation of spheroid formation and invasion capacities with activation of *SNAI1*, which induces epithelial-mesenchymal transition, compared with the control (Fig. 3E and F, Supplementary Fig. 1A).

We further investigated the effect of SALL4 knockdown in HuH7 cells, which intrinsically expressed high levels of SALL4. Expression of *SALL4* was decreased to 50% in HuH7 cells transfected with SALL4 sh-RNA compared with the control when evaluated by qRT-PCR (Fig. 4A). However, the reduction of SALL4 protein was more evident when evaluated by Western blotting, suggesting that this sh-RNA construct might work at the translational as well as the transcriptional level (Fig. 4B). Knock down of *SALL4* resulted in a compromised invasion capacity and spheroid formation capacity with decreased expression of *EPCAM* and *CD44* in HuH7 cells (Fig. 4C and D, Supplementary Fig. 1B and C).

SALL4 and HDAC activity in HpSC-HCC

The above data suggested that SALL4 is a good target and biomarker for the diagnosis and treatment of HpSC-HCCs. However, it is difficult to directly target SALL4 as no studies have investigated the inhibition of its transcription using chemical or other approaches [21]. We therefore re-investigated the interaction networks associated with *SALL4*, and found that SALL4 activation appeared to induce epigenetic modification (Fig. 1B). In particular, a recent study suggested that SALL4 forms a nucleosome remodeling and deacetylase (NuRD) complex with HDACs and potentially regulates HDAC activity [22]. We therefore confirmed that *SALL4* knock down resulted in the reduced activity of total HDAC in HuH7 cells (Fig. 4E). We also evaluated the effect of the overexpression of SALL4 in HuH1 and HLE cells, which do not express SALL4 endogenously, and SALL4 overexpression was found to result in a modest increase of HDAC activity and mild enhancement of chemosensitivity to an HDAC inhibitor SBHA in both cell lines (Supplementary Fig. 2A and B). We further investigated HDAC activity in two SALL4-positive (Hep3B, HuH7) and two SALL4-negative (HLE, HLF) HCC cell lines. Interestingly, high HDAC activities were detected in SALL4-positive compared with SALL4-negative HCC cell lines (Fig. 4F). The HDAC inhibitor SBHA was found to inhibit proliferation of SALL4-positive HCC cell lines at a concentration of 10 μM. By contrast, SBHA had little effect on the proliferation of SALL4-negative HCC cell lines at this concentration (Fig. 4G). SBHA treatment suppressed the expression of SALL4 gene/protein expression in SALL4-positive HuH7 and Hep3B cell lines (Supplementary Fig. 3A and B). We further investigated the effect of SAHA, an additional HDAC inhibitor, in these HCC cell lines, and SAHA was found to more efficiently suppress the cell proliferation of SALL4-positive cell lines compared with SALL4-negative cell lines (Supplementary Fig. 3C).

Taken together, our data suggest a pivotal role for the transcription factor SALL4 in regulating the stemness of HpSC-HCC. SALL4 was detected in HpSC-HCCs with poor prognosis, and inactivation of SALL4 resulted in a reduced invasion/spheroid formation capacity and decreased expression of hepatic stem cell markers. The HDAC inhibitors inhibited proliferation of SALL4-positive HCC cell lines with a reduction of SALL4 gene/protein expression, suggesting their potential in the treatment of SALL4-positive HpSC-HCC.

Discussion

Stemness traits in cancer cells are currently of great interest because they may explain the clinical outcome of patients according to the malignant nature of their tumor. Recently, we

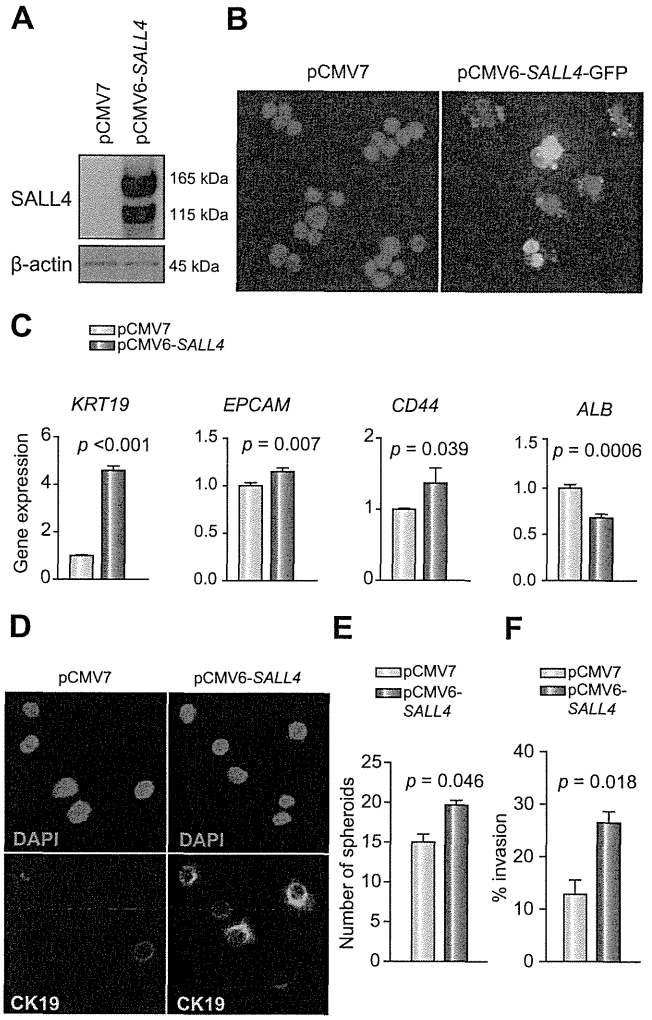

Fig. 3. Effect of SALL4 overexpression. (A) Western blots of cell lysates with anti-SALL4 antibodies. HuH1 cells were transfected with pCMV7 or pCMV6-*SALL4* and incubated for 72 h. (B) IF analysis of HuH1 cells transfected with pCMV7 or pCMV6-*SALL4* and incubated for 72 h. (C) qRT-PCR analysis of *KRT19*, *EPCAM*, *CD44*, and *ALB* in HuH1 cells transfected with pCMV7 or pCMV6-*SALL4* and incubated for 48 h. (D) IF analysis of HuH1 cells transfected with pCMV7 or pCMV6-*SALL4*, incubated for 72 h and stained with anti-CK19 antibodies, evaluated by the confocal laser scanning microscopy. (E) Spheroid formation assay of HuH1 cells transfected with pCMV7 or pCMV6-*SALL4*. Number of spheroids obtained from 2000 cells is indicated (n = 3, mean ± SD). (F) Invasion assay of HuH1 cells transfected with pCMV7 or pCMV6-*SALL4* (n = 3, mean ± SD). (This figure appears in colour on the web.)

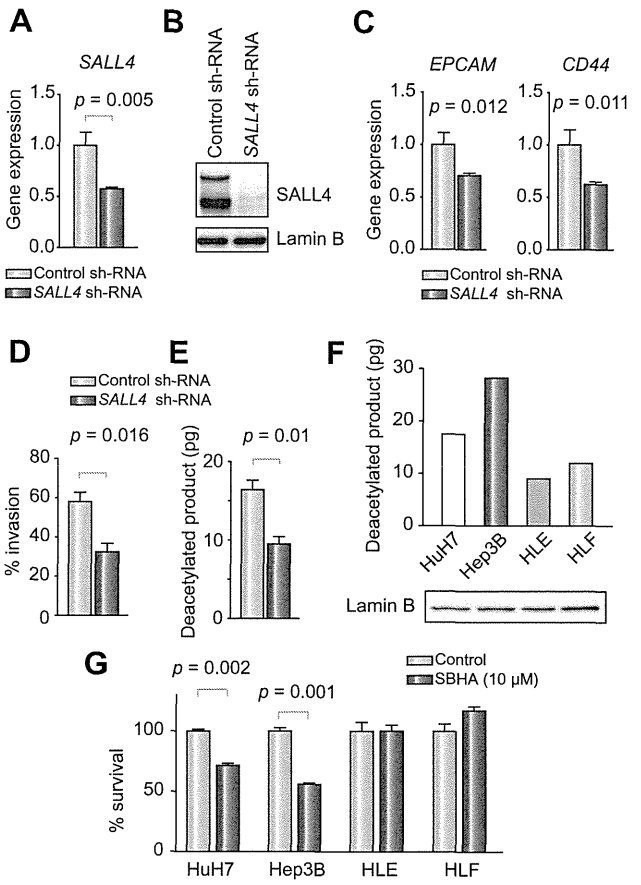

Fig. 4. Effect of *SALL4* knockdown and HDAC activity. (A) qRT-PCR analysis of *SALL4* in HuH7 cells transfected with control or *SALL4* sh-RNAs (n = 3, mean ± SD). (B) Western blots of lysates obtained from HuH7 cells transfected with control or *SALL4* sh-RNAs with anti-SALL4 antibodies. (C) qRT-PCR analysis of *EPCAM* and *CD44* in HuH7 cells transfected with control or *SALL4* sh-RNAs (n = 3, mean ± SD). (D) Invasion assay of HuH7 cells transfected with control or *SALL4* sh-RNAs (n = 3, mean ± SD). (E) HDAC activity of nuclear extracts obtained from HuH7 cells transfected with control or *SALL4* sh-RNAs. (F) HDAC activity of nuclear extracts obtained from each cell line. HDAC activity was measured in duplicate and average amounts of deacetylated products are indicated (upper panel). Lamin B included in the nuclear extracts loaded for HDAC activity assays was measured by Western blotting (lower panel). (G) Cell proliferation assay of HCC cell lines. Each cell line was treated with control DMSO or 10 μM SBHA and cultured for 72 h (n = 4, mean ± SD).

proposed an HCC classification system based on the stem/maturation status of the tumor by EpCAM and AFP expression status [8]. These HCC subtypes showed distinct gene expression patterns with features resembling particular stages of liver lineages. Among them, HpSC-HCC was characterized by a highly invasive nature, chemoresistance to fluorouracil, and poor prognosis after radical resection, warranting the development of a novel therapeutic approach against this HCC subtype [9].

In this study, we showed that the transcription factor SALL4 was activated in HpSC-HCC and that SALL4 might regulate HCC stemness, as characterized by the activation of EpCAM, CK19, and CD44 with highly tumorigenic and invasive natures. Furthermore, we identified that SALL4-positive HCC cell lines tended to show high HDAC activity and chemosensitivity to the HDAC inhibitors SBHA and SAHA. This study reveals for the first time the utility of SBHA for the treatment of HCC with stem cell features.

SALL4 is a zinc finger transcription factor originally cloned based on sequence homology to *Drosophila sal* [11]. *SALL4* mutations are associated with the Okihiro syndrome, a human disease involving multiple organ defects [23,24]. SALL4 plays a fundamental role in the maintenance of embryonic stem cells, potentially through interaction with Oct4, Sox2, and Nanog [25–30]. Furthermore, knockdown of SALL4 significantly reduces the efficiency of induced pluripotent stem cell generation [31]. *SALL4* is also expressed in hematopoietic stem cells and leukemia cells, where it regulates their maintenance [14,32]. SALL4 is known to encode two isoforms (SALL4A and SALL4B), and a recent study

suggested the important role of SALL4B on maintaining the stemness of embryonic stem cells [25]. Interestingly, our data indicated that SALL4B is also a dominant form in HpSC-HCC cell lines. It is unclear how SALL4 isoform expression is regulated in cancer, and future studies are required to explore the mechanisms of SALL4 isoform regulation.

In the liver, SALL4 is expressed in fetal hepatic stem/progenitors but not in adult hepatocytes, and a mouse study demonstrated that inhibition of SALL4 in hepatic stem/progenitors contributes to their differentiation [33]. Interestingly, recent studies indicated that AFP-producing gastric cancer expresses SALL4, suggesting that SALL4 might play a role in the hepatoid differentiation of gastric cancer [34]. Consistently, our data indicated a positive correlation between *SALL4*, *AFP*, and *EPCAM* expression in two independent HCC cohorts. Strikingly, SALL4 was recently shown to be expressed in a subset of human liver cancers with poor prognoses, while modification of SALL4 expression resulted in the alteration of cell proliferation *in vitro* and tumor growth *in vivo*, consistent with our current study [35]. A recent study reported the expression of SALL4 in 46% of HCC cases, which is almost comparable to our present study [36]. Furthermore, a very recent study of two independent large cohorts demonstrated that SALL4 is a marker for a progenitor subclass of HCC with an aggressive phenotype [37]. It is still unclear how SALL4 expression is regulated and which target genes are directly activated by SALL4 binding. Future studies using next generation sequencing are required to fully understand the mechanisms of SALL4 regulation of HCC stemness.

In this study, we demonstrated that SALL4-positive HCC cell lines have high HDAC activity and chemosensitivity against the HDAC inhibitors SBHA and SAHA compared with SALL4-negative HCC cell lines. SALL4 was recently found to directly connect with the epigenetic modulator NuRD complex [22], thereby possibly affecting the histone modification associated with stemness. The NuRD complex is a multiunit chromatin remodeling complex containing chromodomain-helicase-DNA-binding proteins and HDACs that regulate histone deacetylation [38]. Its role in cancer is still controversial, while its function in HCC has not yet been determined.

Our data suggest that SALL4 plays a role in controlling HDAC activity and contributing to the maintenance of HCC with stem cell features. Consistently, HDAC inhibitors might be useful for the eradication of SALL4-positive HCC cells through their inhibitory effects on histone deacetylation by NuRD [39]. Encouragingly, a recent study demonstrated the utility of a SALL4-binding peptide to inhibit its binding to phosphatase and tensin homolog deleted on chromosome 10 (PTEN) through interaction with HDAC, thereby targeting leukemia cells [21]. Further studies are required to understand the relationship between SALL4, the NuRD complex, and the maintenance of stemness in HCC.

Financial support

This study was supported by a Grant-in-Aid from the Ministry of Education, Culture, Sports, Science and Technology, Japan (23590967), a grant from the Japanese Society of Gastroenterology, a grant from the Ministry of Health, Labour and Welfare, and a grant from the National Cancer Center Research and Development Fund (23-B-5), Japan.

Conflict of interest

The authors who have taken part in this study declared that they do not have anything to disclose regarding funding or conflict of interest with respect to this manuscript.

Acknowledgments

We thank Ms. Masayo Baba and Ms. Nami Nishiyama for excellent technical assistance.

Supplementary data

Supplementary data associated with this article can be found, in the online version, at http://dx.doi.org/10.1016/j.jhep.2013.08.024.

References

[1] Nowell PC. The clonal evolution of tumor cell populations. Science 1976;194:23–28.
[2] Hanahan D, Weinberg RA. Hallmarks of cancer: the next generation. Cell 2011;144:646–674.
[3] Jordan CT, Guzman ML, Noble M. Cancer stem cells. N Engl J Med 2006;355:1253–1261.
[4] Clarke MF, Dick JE, Dirks PB, Eaves CJ, Jamieson CH, Jones DL, et al. Cancer stem cells–perspectives on current status and future directions: AACR Workshop on cancer stem cells. Cancer Res 2006;66:9339–9344.
[5] Dean M, Fojo T, Bates S. Tumour stem cells and drug resistance. Nat Rev Cancer 2005;5:275–284.
[6] Visvader JE, Lindeman GJ. Cancer stem cells in solid tumours: accumulating evidence and unresolved questions. Nat Rev Cancer 2008;8:755–768.
[7] Jemal A, Bray F, Center MM, Ferlay J, Ward E, Forman D. Global cancer statistics. CA Cancer J Clin 2011;61:69–90.
[8] Yamashita T, Forgues M, Wang W, Kim JW, Ye Q, Jia H, et al. EpCAM and alpha-fetoprotein expression defines novel prognostic subtypes of hepatocellular carcinoma. Cancer Res 2008;68:1451–1461.
[9] Yamashita T, Ji J, Budhu A, Forgues M, Yang W, Wang HY, et al. EpCAM-positive hepatocellular carcinoma cells are tumor-initiating cells with stem/progenitor cell features. Gastroenterology 2009;136:1012–1024.
[10] Yamashita T, Budhu A, Forgues M, Wang XW. Activation of hepatic stem cell marker EpCAM by Wnt-beta-catenin signaling in hepatocellular carcinoma. Cancer Res 2007;67:10831–10839.
[11] de Celis JF, Barrio R. Regulation and function of spalt proteins during animal development. Int J Dev Biol 2009;53:1385–1398.
[12] Aguila JR, Liao W, Yang J, Avila C, Hagag N, Senzel L, et al. SALL4 is a robust stimulator for the expansion of hematopoietic stem cells. Blood 2011;118:576–585.
[13] Yang J, Chai L, Gao C, Fowles TC, Alipio Z, Dang H, et al. SALL4 is a key regulator of survival and apoptosis in human leukemic cells. Blood 2008;112:805–813.
[14] Yang J, Chai L, Liu F, Fink LM, Lin P, Silberstein LE, et al. Bmi-1 is a target gene for SALL4 in hematopoietic and leukemic cells. Proc Natl Acad Sci U S A 2007;104:10494–10499.
[15] Yamashita T, Honda M, Nio K, Nakamoto Y, Takamura H, Tani T, et al. Oncostatin m renders epithelial cell adhesion molecule-positive liver cancer stem cells sensitive to 5-fluorouracil by inducing hepatocytic differentiation. Cancer Res 2010;70:4687–4697.
[16] Yamashita T, Honda M, Takatori H, Nishino R, Minato H, Takamura H, et al. Activation of lipogenic pathway correlates with cell proliferation and poor prognosis in hepatocellular carcinoma. J Hepatol 2009;50:100–110.
[17] Woo HG, Wang XW, Budhu A, Kim YH, Kwon SM, Tang ZY, et al. Association of TP53 mutations with stem cell-like gene expression and survival of patients with hepatocellular carcinoma. Gastroenterology 2011;140:1063–1070.
[18] Ji J, Wang XW. Clinical implications of cancer stem cell biology in hepatocellular carcinoma. Semin Oncol 2012;39:461–472.

[19] Yang J, Corsello TR, Ma Y. Stem cell gene SALL4 suppresses transcription through recruitment of DNA methyltransferases. J Biol Chem 2012;287: 1996–2005.
[20] Bohm J, Sustmann C, Wilhelm C, Kohlhase J. SALL4 is directly activated by TCF/LEF in the canonical Wnt signaling pathway. Biochem Biophys Res Commun 2006;348:898–907.
[21] Gao C, Dimitrov T, Yong KJ, Tatetsu H, Jeong HW, Luo HR, et al. Targeting transcription factor SALL4 in acute myeloid leukemia by interrupting its interaction with an epigenetic complex. Blood 2013;121:1413–1421.
[22] Lu J, Jeong HW, Kong N, Yang Y, Carroll J, Luo HR, et al. Stem cell factor SALL4 represses the transcriptions of PTEN and SALL1 through an epigenetic repressor complex. PLoS One 2009;4:e5577.
[23] Al-Baradie R, Yamada K, St Hilaire C, Chan WM, Andrews C, McIntosh N, et al. Duane radial ray syndrome (Okihiro syndrome) maps to 20q13 and results from mutations in SALL4, a new member of the SAL family. Am J Hum Genet 2002;71:1195–1199.
[24] Kohlhase J, Heinrich M, Schubert L, Liebers M, Kispert A, Laccone F, et al. Okihiro syndrome is caused by SALL4 mutations. Hum Mol Genet 2002;11:2979–2987.
[25] Rao S, Zhen S, Roumiantsev S, McDonald LT, Yuan GC, Orkin SH. Differential roles of Sall4 isoforms in embryonic stem cell pluripotency. Mol Cell Biol 2010;30:5364–5380.
[26] Tanimura N, Saito M, Ebisuya M, Nishida E, Ishikawa F. Stemness-related factor sall4 interacts with transcription factors oct-3/4 and sox2 and occupies oct-sox elements in mouse embryonic stem cells. J Biol Chem 2013;288:5027–5038.
[27] Wu Q, Chen X, Zhang J, Loh YH, Low TY, Zhang W, et al. Sall4 interacts with nanog and co-occupies nanog genomic sites in embryonic stem cells. J Biol Chem 2006;281:24090–24094.
[28] Yang J, Chai L, Fowles TC, Alipio Z, Xu D, Fink LM, et al. Genome-wide analysis reveals Sall4 to be a major regulator of pluripotency in murine-embryonic stem cells. Proc Natl Acad Sci U S A 2008;105:19756–19761.
[29] Yang J, Gao C, Chai L, Ma Y. A novel SALL4/OCT4 transcriptional feedback network for pluripotency of embryonic stem cells. PLoS One 2010;5:e10766.
[30] Zhang J, Tam WL, Tong GQ, Wu Q, Chan HY, Soh BS, et al. Sall4 modulates embryonic stem cell pluripotency and early embryonic development by the transcriptional regulation of Pou5f1. Nat Cell Biol 2006;8:1114–1123.
[31] Tsubooka N, Ichisaka T, Okita K, Takahashi K, Nakagawa M, Yamanaka S. Roles of Sall4 in the generation of pluripotent stem cells from blastocysts and fibroblasts. Genes Cells 2009;14:683–694.
[32] Yang J, Liao W, Ma Y. Role of SALL4 in hematopoiesis. Curr Opin Hematol 2012;19:287–291.
[33] Oikawa T, Kamiya A, Kakinuma S, Zeniya M, Nishinakamura R, Tajiri H, et al. Sall4 regulates cell fate decision in fetal hepatic stem/progenitor cells. Gastroenterology 2009;136:1000–1011.
[34] Ikeda H, Sato Y, Yoneda N, Harada K, Sasaki M, Kitamura S, et al. Alpha-Fetoprotein-producing gastric carcinoma and combined hepatocellular and cholangiocarcinoma show similar morphology but different histogenesis with respect to SALL4 expression. Hum Pathol 2012;43:1955–1963.
[35] Oikawa T, Kamiya A, Zeniya M, Chikada H, Hyuck AD, Yamazaki Y, et al. SALL4, a stem cell biomarker in liver cancers. Hepatology 2013;57:1469–1483.
[36] Gonzalez-Roibon N, Katz B, Chaux A, Sharma R, Munari E, Faraj SF, et al. Immunohistochemical expression of SALL4 in hepatocellular carcinoma, a potential pitfall in the differential diagnosis of yolk sac tumors. Hum Pathol 2013;44:1293–1299.
[37] Yong KJ, Gao C, Lim JS, Yan B, Yang H, Dimitrov T, et al. Oncofetal gene SALL4 in aggressive hepatocellular carcinoma. N Engl J Med 2013;368: 2266–2276.
[38] Lai AY, Wade PA. Cancer biology and NuRD: a multifaceted chromatin remodelling complex. Nat Rev Cancer 2011;11:588–596.
[39] Marquardt JU, Thorgeirsson SS. Sall4 in "stemness"-driven hepatocarcinogenesis. N Engl J Med 2013;368:2316–2318.

nature medicine

A new cloning and expression system yields and validates TCRs from blood lymphocytes of patients with cancer within 10 days

Eiji Kobayashi[1,4], Eishiro Mizukoshi[2,4], Hiroyuki Kishi[1], Tatsuhiko Ozawa[1], Hiroshi Hamana[1], Terumi Nagai[1], Hidetoshi Nakagawa[2], Aishun Jin[1,3], Shuichi Kaneko[2] & Atsushi Muraguchi[1]

Antigen-specific T cell therapy, or T cell receptor (TCR) gene therapy, is a promising immunotherapy for infectious diseases and cancers. However, a suitable rapid and direct screening system for antigen-specific TCRs is not available. Here, we report an efficient cloning and functional evaluation system to determine the antigen specificity of TCR cDNAs derived from single antigen-specific human T cells within 10 d. Using this system, we cloned and analyzed 380 Epstein-Barr virus–specific TCRs from ten healthy donors with latent Epstein-Barr virus infection and assessed the activity of cytotoxic T lymphocytes (CTLs) carrying these TCRs against antigenic peptide–bearing target cells. We also used this system to clone tumor antigen–specific TCRs from peptide-vaccinated patients with cancer. We obtained 210 tumor-associated antigen–specific TCRs and demonstrated the cytotoxic activity of CTLs carrying these TCRs against peptide-bearing cells. This system may provide a fast and powerful approach for TCR gene therapy for infectious diseases and cancers.

New immunotherapies such as adoptive cell transfer, TCR gene therapy and peptide vaccination have the potential to cure human disease in the future. Rosenberg and his colleagues have reported the adoptive transfer of TCR gene–modified T cells into patients using autologous T cells expressing a TCR recognizing the melanoma-melanocyte differentiation antigen[1,2]. Subsequent clinical trials have targeted antigens such as oncofetal antigen, cancer testis antigen, tissue-specific antigen and overexpressed tumor-associated antigens (TAAs)[3,4]. However, despite its great potential, TCR gene therapy for cancer is still limited to certain tumor antigens and common human leukocyte antigen (HLA) complexes. The conventional approaches for TCR gene cloning involve the establishment of antigen-specific T cell clones, which usually requires several months. Thus, a rapid screening system for antigen-specific TCR genes is needed.

Our group and others have reported single-cell RT-PCR protocols that permit the simultaneous identification of complementarity determining region 3α (CDR3α) and CDR3β transcripts in human[5] and mouse[6] TCRs. However, these protocols cannot retrieve TCRαβ pairs and determine their properties, including antigen specificity and cytotoxicity-inducing activity. In this study, we attempted to establish a direct TCR cloning system that would allow the unbiased analysis of the TCR repertoire, as well as the retrieval of antigen-specific TCRαβ pairs and the characterization of their function for future TCR gene therapy.

RESULTS

Rapid cloning and evaluation of antigen-specific TCRs

We depict the schematic for our rapid cloning and functional assay system, which can obtain TCRαβ cDNA pairs from a single antigen-specific human T cell and confirm their antigen specificity within 10 d (**Fig. 1** and **Supplementary Fig. 1**). This system was designated 'hTEC10' (human TCR efficient cloning within 10 d).

To evaluate the hTEC10 system for analyzing T cells in human disease, we first analyzed Epstein-Barr virus (EBV)-specific $CD8^+$ T cells derived from healthy HLA-$A24^+$ donors with latent EBV infection. We used an HLA-A*2402–restricted major histocompatibility complex (MHC) tetramer mixture of five EBV epitopes (BRLF-1, BMLF-1, latent membrane protein 2 (LMP2), Epstein-Barr nuclear antigen 3A (EBNA3A) and EBNA3B)[7] to detect EBV-specific $CD8^+$ T cells. We detected varying frequencies (0.00–0.64%) of tetramer-positive cells within the $CD8^+$ T cell populations from 19 HLA-$A24^+$ donors (**Fig. 2a** and **Supplementary Table 1**). We then used FACS to sort single tetramer-positive cells from ten donors whose frequencies of tetramer-positive cells were more than 0.06% of $CD8^+$ T cells (with donor I having the minimum frequency of 0.06%). The efficacy of amplifying the TCRα and TCRβ cDNA pairs from the sorted single T cells was 13–72%, using the 5′ rapid amplification of cDNA ends (RACE) method[5] (**Supplementary Table 2**).

We then analyzed the obtained TCR pairs from each donor. A small population expressed dual TCRα, dual TCRβ or both. In some donors, a large number of T cells expressed dual TCRα or dual TCRβ. This may be due to clonal expansion (**Supplementary Table 3**). In total, we obtained 380 EBV-specific TCRs from ten healthy donors with latent EBV infection (**Supplementary Table 2**).

The diversity of the EBV-specific TCRs was highly restricted (from one to ten in each donor) (**Fig. 2b** and **Supplementary Fig. 2**). Because

[1]Department of Immunology, Graduate School of Medicine and Pharmaceutical Sciences, University of Toyama, Toyama, Japan. [2]Department of Gastroenterology, Graduate School of Medicine, Kanazawa University, Kanazawa, Ishikawa, Japan. [3]College of Basic Medical Science, Harbin Medical University, Harbin, China. [4]These authors contributed equally to this work. Correspondence should be addressed to H.K. (immkishi@med.u-toyama.ac.jp).

Received 2 April 2012; accepted 8 April 2013; published online 13 October 2013; doi:10.1038/nm.3358

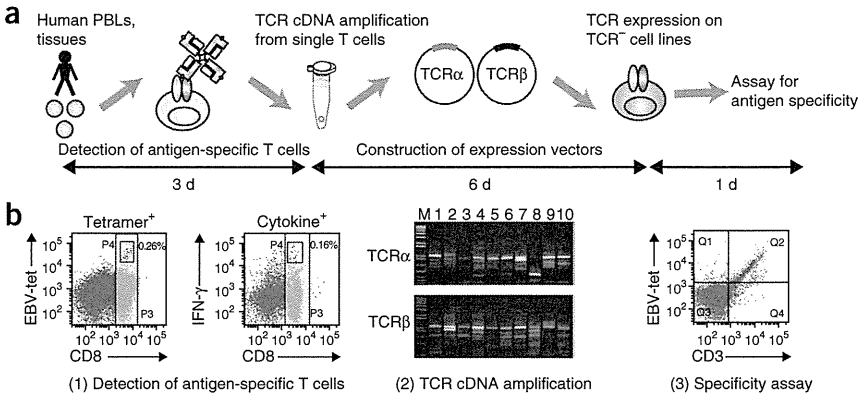

Figure 1 Schematic of the hTEC10 system. (**a**) A schematic depicting the procedure of the hTEC10 system. Briefly, human TCR cDNAs were amplified from single cells, cloned into an expression vector and then transduced into the TCR-negative T cell line TG40. The antigen specificity of TCRs was then assessed by staining the TG40 cells with MHC tetramers or by monitoring CD69 expression. The entire process can be performed within 10 d. (**b**) Detection of antigen-specific T cells with MHC tetramers (left) or cytokine secretion (right) (1), analysis of amplified TCRαβ chain cDNA (2) and examination of TCR expressed on TG40 cells using EBV tetramer (EBV-tet) binding (3).

the TCR repertoire of the tetramer-negative cells was not skewed toward a particular TCRα V or TCRβ V subgroup (**Supplementary Fig. 3**), the skewing of the TCR repertoire in the tetramer-positive cells was not due to PCR bias. Notably, our system can clone rare antigen-specific T cell clones (indicated by asterisks in **Fig. 2b** and **Supplementary Fig. 2**) that may be missed when using conventional cloning methods.

To determine the antigen specificity of the cloned TCRs, we first transferred the cDNA into TG40 cells and stained the cells with MHC-peptide tetramer mixture. The tetramer mixture bound to 95% of the cloned TCRs that were expressed on the TG40 cells (**Fig. 2c**). We then determined the antigenic peptide specificity of the cloned TCRs by stimulating the TCR-expressing TG40 cells with HLA-A24⁺ PBLs that were pulsed with each of the EBV peptides (BRLF-1, BMLF-1, LMP2, EBNA3A or EBNA3B), followed by examining the cell-surface expression of CD69 with flow cytometry. The percentages of TCRs specific for BRLF-1, BMLF-1, EBNA3A, EBNA3B and LMP-2 among the EBV-specific TCRs were 65.5%, 12.6%, 19.7%, 1.6% and 0.5%, respectively (**Fig. 2d** and **Supplementary Table 4**).

EBV-specific TCR cDNA–transduced T cells kill target cells

To determine the cytotoxic activity of EBV-specific TCR cDNA–transduced T cells, we transduced cDNAs encoding BRLF-1–specific

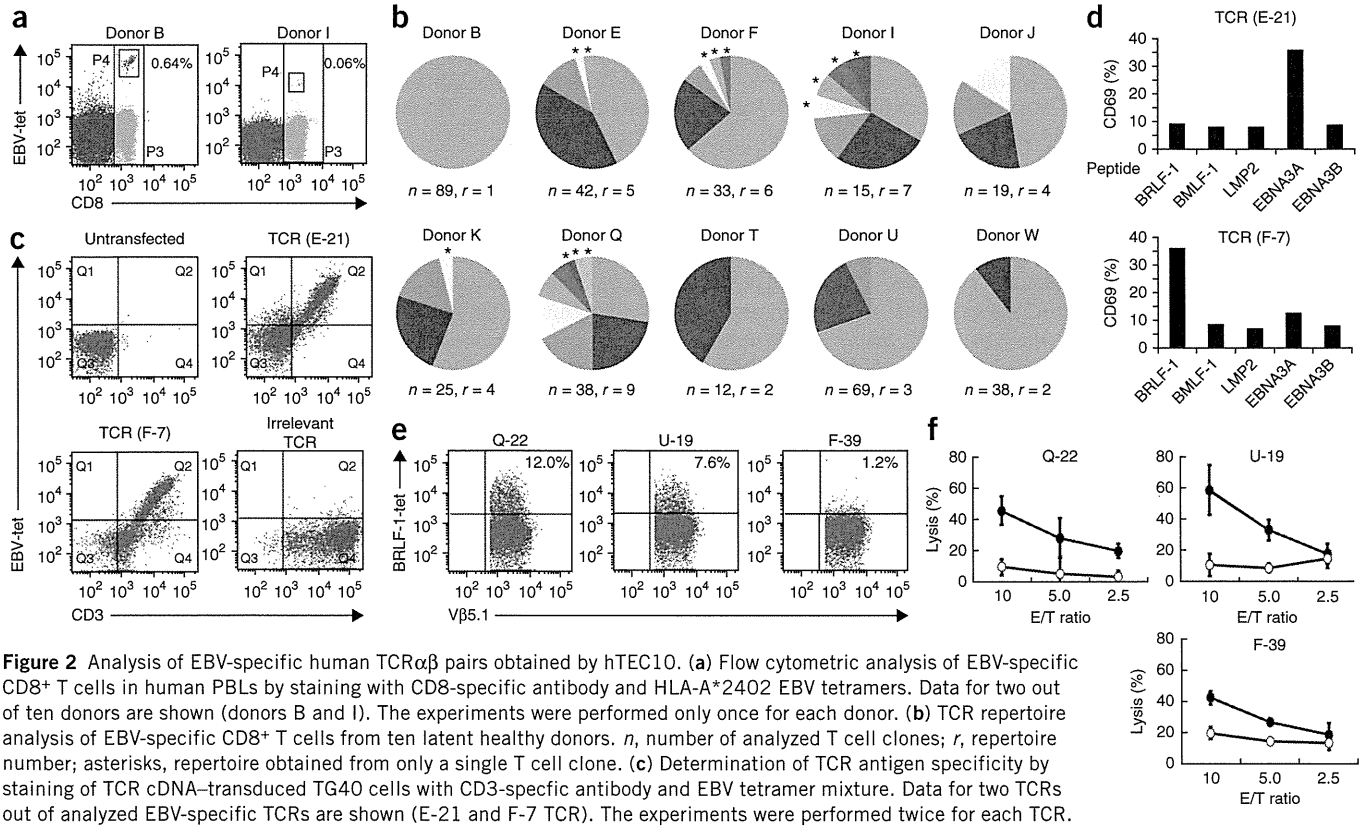

Figure 2 Analysis of EBV-specific human TCRαβ pairs obtained by hTEC10. (**a**) Flow cytometric analysis of EBV-specific CD8⁺ T cells in human PBLs by staining with CD8-specific antibody and HLA-A*2402 EBV tetramers. Data for two out of ten donors are shown (donors B and I). The experiments were performed only once for each donor. (**b**) TCR repertoire analysis of EBV-specific CD8⁺ T cells from ten latent healthy donors. *n*, number of analyzed T cell clones; *r*, repertoire number; asterisks, repertoire obtained from only a single T cell clone. (**c**) Determination of TCR antigen specificity by staining of TCR cDNA–transduced TG40 cells with CD3-specfic antibody and EBV tetramer mixture. Data for two TCRs out of analyzed EBV-specific TCRs are shown (E-21 and F-7 TCR). The experiments were performed twice for each TCR. (**d**) Flow cytometric analysis of CD69 expression in TG40 cells expressing E-21 or F-7 TCRs in the presence of various EBV-derived peptides and HLA-A24⁺ PBLs. (**e**) TCR expression analysis of BRLF-1–specific Vβ5.1⁺ TCRs (Q-22, U-19 or F-39) on TCR cDNA–transduced primary T cells by staining with Vβ5.1-specific antibody and BRLF-1–specific tetramer (BRLF-1-tet). Profile of only Vβ5.1⁺ population is shown. The percentage of Vβ5.1 was 15.4%, 19.1% and 16.9% of PBLs for Q-22, U-19 and F-39, respectively. The percentage of tetramer-positive cells in Vβ5.1⁺ cell population is indicated. Representative data of three independent experiments are shown. (**f**) Cytotoxicity of TCR cDNA–transduced primary T cells against T2-A24 cells pulsed with BRLF-1 peptide (closed circle) or EBNA3A peptide (open circle) labeled with calcein. The results shown are mean ± s.d. of triplicate experiments. E/T ratio, ratio of effector T cells to target cells.

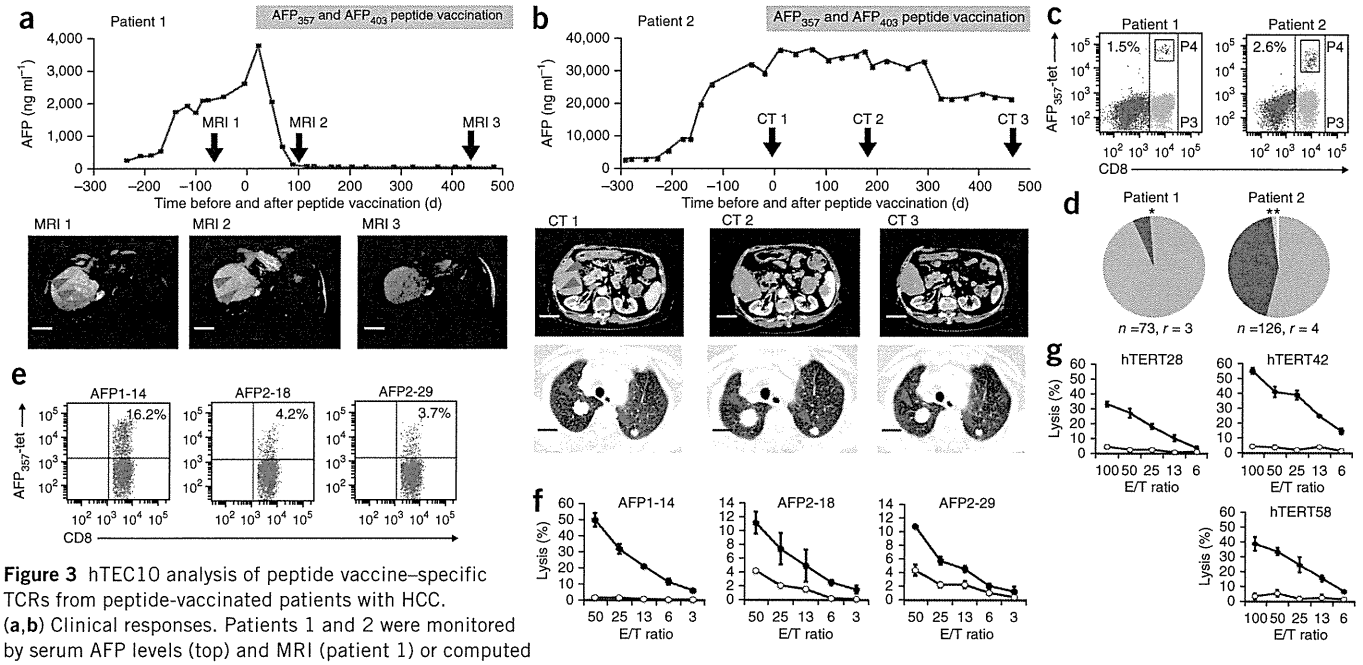

Figure 3 hTEC10 analysis of peptide vaccine–specific TCRs from peptide-vaccinated patients with HCC. (**a**,**b**) Clinical responses. Patients 1 and 2 were monitored by serum AFP levels (top) and MRI (patient 1) or computed tomography (patient 2) (bottom). Black arrows show examination dates and red arrowheads show metastatic lesions of HCC. Scale bars in **a**, 50 mm; in **b**, 50 mm (top) and 30 mm (bottom). (**c**) Detection of AFP_{357} peptide–specific $CD8^+$ T cells of PBLs in patients with HCC with CD8-specific antibody and AFP_{357}-specific tetramers. Percentages of AFP_{357}-specific tetramer-positive cells in $CD8^+$ T cells are indicated. (**d**) Repertoire of AFP_{357} $tetramer^+$ $CD8^+$ T cells. *n*, number of analyzed T cell clones; *r*, repertoire number; asterisk, repertoire obtained from only a single T cell clone. (**e**) Expression of AFP_{357}-specific TCRs on TCR cDNA–transduced primary T cells. Profile of only $CD8^+$ population is shown. Percentages of AFP_{357}-specific tetramer-positive cells among $CD8^+$ T cells are indicated. (**f**) Cytotoxicity of AFP-specific TCR cDNA–transduced primary T cells toward C1R-A24 cells pulsed with AFP_{357}-peptide (closed circle) or control peptide (open circle). Data are expressed as mean ± s.d. of triplicate experiments. Representative data of three independent experiments are shown. (**g**) Cytotoxicity of hTERT–specific TCR cDNA–transduced primary T cells toward C1R-A24 cells pulsed with $hTERT_{461}$ peptide (closed circle) or control peptide (open circle). Data are expressed as mean ± s.d. of triplicate experiments. Representative data of three independent experiments are shown.

Vβ5.1$^+$ TCRs (clones Q-22, U-19 and F-39) into primary human T cells using retroviral vectors and compared their ability to kill T2-A24 cells, a TAP-deficient T2 cell line expressing HLA-A*2402 (ref. 8), that had been pulsed with the BRLF-1 peptide. These three TCRs have the same Vβ region (Vβ5.1$^+$) but distinct CDR3 sequences and Vα regions. The BRLF-1 tetramer bound to 12.0%, 7.6% and 1.2% of Vβ5.1$^+$ cells in the T cell populations that were transduced with Q-22, U-19 and F-39 TCR cDNAs, respectively, whereas the percentages of Vβ5.1$^+$ cells in the Q-22, U-19 and F-39 TCR cDNA transfectants were the same level (**Fig. 2e** and **Supplementary Fig. 4a**). This result indicates that the transduced TCRs tend to mispair with endogenous TCRs[9].

We then determined the cytotoxic activity of T cells that were transduced with the BRLF-1–specific TCR cDNAs against T2-A24 cells that had been pulsed with the BRLF-1 or the EBNA3A peptide. T cells transduced with BRLF-1–specific TCR cDNAs exhibited cytotoxicity toward the BRLF-1 peptide–pulsed T2-A24 cells but not toward the EBNA3A peptide–pulsed cells (**Fig. 2f**), demonstrating that the cytotoxic activity was peptide specific. Similarly, T cells transduced with EBNA3A-specific TCR (E-21) cDNAs demonstrated cytotoxicity toward EBNA3A peptide–pulsed T2-A24 cells but not BRLF-1 peptide–pulsed cells (**Supplementary Fig. 5a**,**c**).

We also measured the cytokine secretion of the TCR cDNA–transduced T cells after antigen stimulation. Peripheral blood lymphocytes (PBLs) transduced with BRLF-1–specific TCR cDNAs (Q-22, U-19 and F-39) secreted multiple cytokines (interferon-γ (IFN-γ), tumor necrosis factor-α (TNF-α) and interleukin-2 (IL-2)) upon stimulation with the BRLF-1 peptide, but not with the EBNA3A peptide (**Supplementary Fig. 6**). In contrast, PBLs transduced with the EBNA3A-specific TCR (E-21) cDNAs secreted IFN-γ upon stimulation with the EBNA3A peptide but with the BRLF-1 peptide (**Supplementary Fig. 5b**).

Furthermore, we examined the functional avidity of the EBV-specific TCRs using the TG40-based TCR downregulation assay, and we determined the half-maximum inhibitory concentration (IC_{50}) of the peptide responses. The Q-22 TCR exhibited the highest functional avidity (**Supplementary Fig. 7** and **Supplementary Table 5**). Therefore, we examined whether T cells transduced with the Q-22 TCR cDNA could respond to EBV-transformed lymphoblastoid cell line (LCL) cells endogenously expressing the EBV antigen and HLA-A*2402 (JTK-LCL cells). The Q-22 TCR cDNA–transduced T cells exhibited a marked response to JTK-LCL cells and produced IFN-γ (**Supplementary Fig. 8**). However, we did not detect CTL activity of the Q-22 TCR cDNA–transduced T cells against JTK-LCL cells. These data are in agreement with a previous report[7]. This lack of cytotoxicity may be owing to limited presentation of the BRLF-1 peptide by HLA-A*2402 on the cell surface of JTK-LCL cells.

In summary, we obtained 380 EBV-specific TCRαβ cDNA pairs and analyzed the TCR repertoires. All of the cloned TCRs were previously uncharacterized (**Supplementary Table 6**).

Clinical application of hTEC10 system in people with cancer

To apply the hTEC10 system to patients with cancer, we obtained PBLs from two patients with hepatocellular carcinoma (HCC) who had been treated with α-fetoprotein (AFP)-derived peptide vaccines and exhibited clinical responses. We show the clinical courses of cancer in these patients (**Fig. 3a**,**b**). The first patient (patient 1), who was infected with hepatitis B virus (HBV) and had a large HCC tumor with vascular invasion of

the portal vein, was vaccinated with the AFP_{357} and AFP_{403} peptides biweekly for 72 weeks. After vaccination, the patient's elevated serum AFP value was normalized; the size of the HCC tumor also decreased, and it eventually disappeared, as evaluated by magnetic resonance imaging (MRI) (**Fig. 3a**), indicating a complete response. The second patient (patient 2), who was infected with HBV and had multiple metastatic HCC lesions in the abdominal wall and lungs, was vaccinated with the AFP_{357} and AFP_{403} peptides biweekly for 88 weeks. After vaccination, the patient's elevated serum AFP value decreased, and the metastatic HCC lesions in the abdominal wall disappeared, as evaluated by computed tomography (**Fig. 3b**). The size and number of lung metastases did not change over the 88 weeks of treatment, indicating stable disease.

We examined whether AFP_{357}-specific T cells could be detected in the PBLs of patients 1 and 2 before or during vaccination by employing an AFP_{357}-specific tetramer and flow cytometry. We could not detect AFP-specific $CD8^+$ T cells detected in the PBLs of the patients either before or during treatment (**Supplementary Fig. 9**). However, when we incubated the PBLs with AFP-derived peptides for 3 weeks to expand the AFP-specific $CD8^+$ T cells, we detected AFP_{357}-specific T cells in the PBLs obtained from both patients during vaccination but not from the PBLs obtained before vaccination (**Supplementary Fig. 10**). These data indicate that the detection of AFP_{357}-specific TCRs in the patients' PBLs was due to peptide vaccination.

1.5% and 2.6% of the $CD8^+$ T cells were positive for tetramer staining in patients 1 and 2, respectively (**Fig. 3c**). We then sorted the single AFP tetramer–positive $CD8^+$ T cells, amplified the TCR cDNAs and analyzed their sequences. We obtained 73 and 126 AFP-specific TCRs from patients 1 and 2, respectively. The sequence analysis revealed that the hTEC10 system yielded three and four T cell clones from patients 1 and 2, respectively (**Fig. 3d**), suggesting that peptide vaccination induced the oligoclonal expansion of AFP-specific T cells in these patients. Alternatively, *in vitro* culture may have resulted in the oligoclonal expansion of AFP-specific T cells. In contrast to EBV-specific TCRs, the repertoires of AFP-specific TCRs might be biased by *in vitro* culture, as suggested by Zhou *et al.*[10]. Notably, the hTEC10 system could clone TCRs from very rare antigen-specific T cells, as in the case of EBV-specific minor clones (**Fig. 3d**).

We then transduced three of the obtained AFP-specific TCR cDNAs into primary T cells of a healthy donor and analyzed the binding of the AFP tetramer. The TCR cDNAs were transduced into 28–32% of the T cells (**Supplementary Fig. 4b**), and 3.7–16.2% of the total $CD8^+$ cells bound the AFP tetramer (**Fig. 3e**). We then determined the cytotoxic activity of the transduced T cells toward C1R-A24 cells (an LCL transfected with HLA-A*2402)[11] pulsed with the AFP peptide. The T cells transduced with these TCR cDNAs showed marked cytotoxicity toward AFP peptide–pulsed C1R-A24 cells but not control peptide ($HIV_{584-592}$)-pulsed cells (**Fig. 3f**), indicating that the cytotoxic activity was peptide specific. We also measured cytokine secretion by the TCR cDNA–transduced T cells after antigen stimulation. PBLs transduced with AFP_{357}-specific TCR cDNAs (AFP1-14, AFP2-28 and AFP2-29), but not PBLs transduced with control GFP vector, secreted IFN-γ when stimulated with the AFP_{357} peptide (**Supplementary Fig. 11**).

Next, we examined the cytotoxic activity of the T cells transduced with AFP-specific TCR cDNAs to HepG2 cells, which endogenously express AFP[11]. However, they did not show any specific cytotoxicity to the target cells (data not shown). We also obtained four kinds of human telomerase reverse transcriptase (hTERT)-specific TCRs from patients with HCC who had been vaccinated with hTERT peptide in the clinical trial (**Supplementary Fig. 12**). We transduced three hTERT-specific TCR cDNAs in primary T cells and examined their cytotoxic activity toward

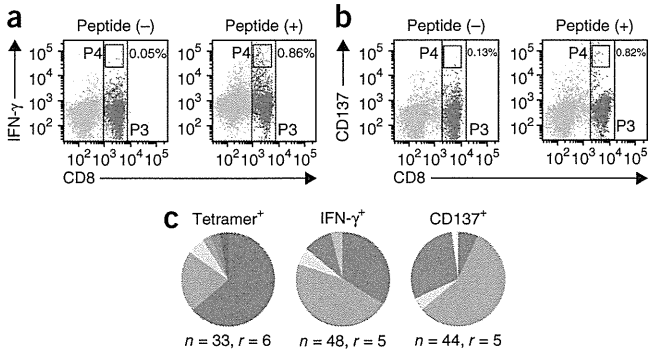

Figure 4 Repertoire analysis of cytokine-secreting $CD8^+$ T cells by stimulation with a specific peptide. (**a**) Secretion of IFN-γ by BRLF-1 peptide–stimulated PBLs. Percentages of IFN-γ–secreting cells in $CD8^+$ T cells are indicated. (**b**) Upregulation of CD137 on BRLF-1 peptide–stimulated PBLs. (**c**) Repertoires of IFN-γ$^+$ $CD8^+$ T cells and $CD137^+$ $CD8^+$ T cells. *n*, number of analyzed T cell clones; *r*, repertoire number. The same color denotes the same Vα or Vβ repertoires.

hTERT peptide–pulsed C1R-A24 cells or HepG2 cells that endogenously expressed hTERT. The T cells transduced with human TERT–specific TCR cDNAs (hTERT28, hTERT42 and hTERT58) showed marked cytotoxicity toward hTERT peptide–pulsed C1R-A24 cells (**Fig. 3g**). However, they did not show marked cytotoxicity toward HepG2 cells (data not shown). These results demonstrate that the hTEC10 system can clone functional TAA peptide–specific TCRs from patients with cancer.

Improvement of the hTEC10 system

We next established new MHC tetramer-independent systems to clone TCR cDNAs using cytokine secretion and CD137 upregulation. We obtained PBLs from healthy donors with latent EBV infection and incubated these cells with the BRLF-1 peptide to expand the BRLF-1–specific $CD8^+$ T cells *in vitro*. We then stimulated the expanded BRLF-1–specific $CD8^+$ T cells in the presence of CD28-specific antibody with or without the BRLF-1 peptide and examined IFN-γ secretion or CD137 upregulation. 0.86% of the $CD8^+$ T cells were IFN-γ positive, and 0.82% of the $CD8^+$ T cells had upregulated CD137 (**Fig. 4a,b**). We then sorted the single T cells and analyzed their TCR sequences. We obtained 48 TCRs from the IFN-γ–secreting cells and 44 TCRs from the CD137-upregulated cells, and we compared the repertoires of these populations with those obtained from the MHC-peptide tetramer staining method (**Fig. 4c**).

We found that 86% of the TCR repertoire of the IFN-γ–positive T cells and 68% of that for the CD137-upregulated T-cells was identical to that identified by staining with the MHC-peptide tetramer. We also tested the tetramer-binding ability of five TCR clones that were isolated with the IFN-γ–based protocol and five TCR clones that were isolated with the CD137 upregulation protocol. All of the clones bound the tetramer (data not shown). In addition, we examined the ability of six TCRs that bound the MHC-peptide tetramer (**Supplementary Fig. 13**) to induce IFN-γ production when transduced into PBLs. All six TCR cDNA–transduced PBLs produced IFN-γ (**Supplementary Fig. 14**). Taken together, these results demonstrate that the hTEC10 system can rapidly and efficiently clone TCR cDNAs by assessing cytokine secretion or CD137 upregulation.

DISCUSSION

In this study, we established a system for the rapid and direct cloning and functional evaluation of TCR cDNAs derived from single antigen-specific

human T cells (hTEC10 system). We used this system to obtain and analyze antigen-specific TCRs from healthy donors and patients with cancer.

With regard to minimal frequencies of specific T cells required for the proper identification of TCRs, the frequency of the EBV tetramer$^+$ cells of donor I was the minimum (0.06% of the CD8$^+$ T cells or 0.01% of the total PBLs). We sorted 48 EBV tetramer$^+$ cells from 8×10^6 cells. Twenty-three pairs of TCR α and β cDNAs were amplified. Fifteen of them could be expressed in TG40 cells and could bind EBV tetramer.

Regarding the processing time, the hTEC10 system can obtain antigen-specific TCR cDNAs within 10 d when the antigen-specific T cells are detected on day 1. If the antigen-specific T cells cannot be detected in primary T cells, they need to be cultured for a certain duration. Thus, 8 d, plus additional days for *in vitro* culture, are required to obtain antigen-specific TCRs.

Concerning the EBV-specific TCR repertoires, all of the cloned TCRs were previously uncharacterized. The repertoire of EBV-specific TCRs was highly restricted, in agreement with previous reports[12,13]. The analysis was reproducible, as we obtained similar results from donor B and donor E in two independent experiments.

To determine candidate TCRs for gene therapy for cancer, we used the hTEC10 system to analyze PBLs derived from patients with HCC who had been successfully treated by AFP-derived peptide vaccination. The appropriateness of oncofetal antigens as targets for TCR gene therapy has recently been questioned[14]. However, Butterfield *et al.*[15] previously reported that a phase 1/2 clinical trial of immunization with dendritic cells pulsed with HLA-A*0201–restricted AFP peptides in patients with HCC showed no adverse events. Furthermore, we previously compared the *in vitro* effect of various TAA peptides on PBLs from patients with HCC and showed that HLA-A*2402–restricted AFP peptides may be candidates for peptide vaccination of patients with HCC[11,16]. Thus, a clinical trial to determine the effectiveness of AFP-derived peptide vaccination for patients with HCC has already been conducted, and several patients have exhibited positive clinical responses.

Our data showed that primary T cells transduced with AFP-specific and hTERT-specific TCR cDNAs showed potent antigen-specific cytotoxicity toward AFP- or hTERTpeptide–pulsed target cells, but they did not show marked cytotoxicity toward HepG2 cells that had been reported to endogenously express AFP and hTERT (data not shown). We reasoned three possibilities. The first is that the efficiencies of TCR transduction into PBLs were low. The second is that HepG2 cells may present an insufficient amount of hTERT peptide on their HLA-A24 molecules. The third is the weak affinity of the obtained TCRs. We need to clone more AFP- and hTERT-specific TCRs to acquire TCRs with sufficient affinity to induce cytotoxicity toward HepG2 cells.

Finally, we applied the hTEC10 system to detect and retrieve TCRαβ pair cDNAs by analyzing cytokine secretion and CD137 upregulation. Most of the TCR repertoire of IFN-γ–positive T cells or CD137-upregulated T cells was identical to that identified by the MHC-peptide tetramer, whereas the rest were not identical. These results, along with the CD69 induction assay, indicate that the hTEC10 system can be used with cytokine-secreting or CD137-upregulated CD8$^+$ T cells without the need for staining with an MHC-peptide multimer. Therefore, we can apply the hTEC10 system to isolate T cells from patients with cancer for whom the identity of the tumor antigen is unknown. The T cells can be stimulated with tumor cells, and the IFN-γ–secreting or CD137-upregulated CD8$^+$ cells can be sorted. After cloning the TCRs, their specificity can be examined by analyzing the response of TCR cDNA–transduced T cells to the tumor cells.

METHODS

Methods and any associated references are available in the online version of the paper.

Accession codes. cDNA sequences were deposited in DNA Data Bank of Japan with accession codes from AB749820 to AB749925.

Note: Any Supplementary Information and Source Data files are available in the online version of the paper.

ACKNOWLEDGMENTS

We thank S. Hirota, A. Takishita, K. Shitaoka and M. Horii for technical assistance and K. Hata for secretarial work. This research was supported by grants from the Hokuriku Innovation Cluster for Health Science and a Grant-in-Aid from the Ministry of Education, Culture, Sports, Science and Technology in Japan (11F01415 and 24650630). Retroviral pMX vector, pMX-IRES-EGFP vector and PLAT-E cell line were kindly provided by T. Kitamura (University of Tokyo), human CD8–expressing TG40 cell line by T. Ueno and C. Motozono (Kumamoto University) with permission from T. Saito (Riken), T2-A24 cell line by K. Kuzushima (Aichi Cancer Center Research Institute), Phoenix-A cell line by G. Nolan (Stanford University) and C1R-A24 cell line from M. Takiguchi (Kumamoto University).

AUTHOR CONTRIBUTIONS

E.K., E.M., H.H., T.N. and A.J. performed and analyzed the experiments. E.K., E.M., H.K., S.K., H.N. and A.M. designed the experiments. E.M. and T.O. contributed reagents. E.K., H.K. and A.M. wrote the manuscript, and E.K., E.M., H.K., S.K. and A.M. edited the manuscript.

COMPETING FINANCIAL INTERESTS

The authors declare no competing financial interests.

1. Morgan, R.A. *et al.* Cancer regression in patients after transfer of genetically engineered lymphocytes. *Science* **314**, 126–129 (2006).
2. Johnson, L.A. *et al.* Gene therapy with human and mouse T-cell receptors mediates cancer regression and targets normal tissues expressing cognate antigen. *Blood* **114**, 535–546 (2009).
3. Linnemann, C., Schumacher, T.N. & Bendle, G.M. T-cell receptor gene therapy: critical parameters for clinical success. *J. Invest. Dermatol.* **131**, 1806–1816 (2011).
4. Uttenthal, B.J., Chua, I., Morris, E.C. & Stauss, H.J. Challenges in T cell receptor gene therapy. *J. Gene Med.* **14**, 386–399 (2012).
5. Ozawa, T., Tajiri, K., Kishi, H. & Muraguchi, A. Comprehensive analysis of the functional TCR repertoire at the single-cell level. *Biochem. Biophys. Res. Commun.* **367**, 820–825 (2008).
6. Dash, P. *et al.* Paired analysis of TCRα and TCRβ chains at the single-cell level in mice. *J. Clin. Invest.* **121**, 288–295 (2011).
7. Kuzushima, K. *et al.* Tetramer-assisted identification and characterization of epitopes recognized by HLA A*2402-restricted Epstein-Barr virus-specific CD8$^+$ T cells. *Blood* **101**, 1460–1468 (2003).
8. Miyahara, Y. *et al.* Determination of cellularly processed HLA-A2402–restricted novel CTL epitopes derived from two cancer germ line genes, MAGE-A4 and SAGE. *Clin. Cancer Res.* **11**, 5581–5589 (2005).
9. Okamoto, S. *et al.* Improved expression and reactivity of transduced tumor-specific TCRs in human lymphocytes by specific silencing of endogenous TCR. *Cancer Res.* **69**, 9003–9011 (2009).
10. Zhou, J., Dudley, M.E., Rosenberg, S.A. & Robbins, P.F. Selective growth, *in vitro* and *in vivo*, of individual T cell clones from tumor-infiltrating lymphocytes obtained from patients with melanoma. *J. Immunol.* **173**, 7622–7629 (2004).
11. Mizukoshi, E., Nakamoto, Y., Tsuji, H., Yamashita, T. & Kaneko, S. Identification of α-fetoprotein–derived peptides recognized by cytotoxic T lymphocytes in HLA-A24$^+$ patients with hepatocellular carcinoma. *Int. J. Cancer* **118**, 1194–1204 (2006).
12. Lim, A. *et al.* Frequent contribution of T cell clonotypes with public TCR features to the chronic response against a dominant EBV-derived epitope: application to direct detection of their molecular imprint on the human peripheral T cell repertoire. *J. Immunol.* **165**, 2001–2011 (2000).
13. Argaet, V.P. *et al.* Dominant selection of an invariant T cell antigen receptor in response to persistent infection by Epstein-Barr virus. *J. Exp. Med.* **180**, 2335–2340 (1994).
14. Parkhurst, M.R. *et al.* T cells targeting carcinoembryonic antigen can mediate regression of metastatic colorectal cancer but induce severe transient colitis. *Mol. Ther.* **19**, 620–626 (2011).
15. Butterfield, L.H. *et al.* A phase I/II trial testing immunization of hepatocellular carcinoma patients with dendritic cells pulsed with four α-fetoprotein peptides. *Clin. Cancer Res.* **12**, 2817–2825 (2006).
16. Mizukoshi, E. *et al.* Comparative analysis of various tumor-associated antigen-specific T-cell responses in patients with hepatocellular carcinoma. *Hepatology* **53**, 1206–1216 (2011).

ONLINE METHODS

Healthy donors and human leukocyte antigen typing. Human experiments were performed with the approval of the Ethical Committee at the University of Toyama, Toyama, Japan. Informed consent was obtained from all subjects. PBLs were isolated as described previously[16]. HLA-A24 and HLA-A02 haplotype positivity was screened by staining PBLs with FITC-conjugated HLA-A24 (clone 17A10) and HLA-A2 (clone BB7.2) antibody (MBL) and analyzed with flow cytometry.

Peptide vaccination of patients. The clinical trial of the HLA-A24–restricted AFP_{357} (EYSRRHPQL) and AFP_{403} (KYIQESQAL) peptide vaccines (trial registration: UMIN000003514) and that of the HLA-A24–restricted $hTERT_{461}$ (VYGFVRACL) peptide vaccines (trial registration: UMIN000003511) were conducted at Kanazawa University Hospital, Kanazawa, Japan. Patients with verified radiological diagnoses of HCC stage III or IV were enrolled in this study. The patients each received 3.0 mg of AFP-derived peptide vaccine in each dose. The peptides, which were synthesized as GMP-grade products at Neo MPS, were administered as an emulsified solution containing incomplete Freund's adjuvant (Montanide ISA-51 VG; SEPPIC) by biweekly subcutaneous immunization for 72 weeks (patient 1) and 88 weeks (patient 2). Clinical responses were monitored by measuring the serum AFP value and carrying out dynamic computed tomography or MRI and were evaluated according to the Response Evaluation Criteria in Solid Tumors, version 1.1. All patients provided written informed consent to participate in the study in accordance with the Helsinki Declaration, and this study was approved by the regional ethics committee (Medical Ethics Committee of Kanazawa University, No. 858). Blood samples from the patients were tested for the surface antigen of the HBV and hepatitis C virus using commercial immunoassays (Fuji Rebio). HLA-based typing of patient PBLs was performed using the polymerase chain reaction–reverse sequence-specific oligonucleotide (PCR-RSSO) method. The serum AFP level was measured by ELISA (Abbott Japan). PBLs were isolated from patients as described previously[16], resuspended in RPMI 1640 medium containing 80% FCS and 10% dimethyl sulfoxide and cryopreserved until use.

Cell culture and cell lines. RPMI 1640 and DMEM media (Wako Pure Chemical) were supplemented with 10% FBS (Biowest), 100 μg ml^{-1} streptomycin and 100 U ml^{-1} penicillin. Human CD8-expressing TG40 cells[17], T2-A24 cells[8] from a transporter associated with antigen presentation (TAP)-deficient T2 cell line transfected with HLA-A*2402 and C1R-A24 cells from a C1R lymphoblastoid cell line transfected with HLA-A*2402 (ref. 11) were maintained in RPMI 1640 medium. PLAT-E[18] and Phoenix-A[19] (a retroviral packaging cell line) and HepG2, (hepatocellular carcinoma cell line, purchased from ATCC), were maintained in DMEM medium.

Antibody and MHC tetramer staining. FITC-conjugated CD8-specific antibody (1: 200, clone T8) and PC5-conjugated CD8-specific antibody (1: 1,000, clone B9.11) were purchased from Beckman Coulter. Phycoerythrin-conjugated CD137-specific antibody (1:40, clone 4B4-1) was purchased from BioLegend. Biotin-conjugated CD3ε-specific antibody (1:200, clone 145-2C11), allophycocyanin-conjugated streptavidin and phycoerythrin-conjugated CD69-specific antibody (1:200, clone H1.2F3) were purchased from eBioscience. EBV-specific T cells were stained with phycoerythrin-conjugated HLA-A*2402–peptide tetramers or HLA-A*0201–peptide tetramers. The sequences of the HLA-A*2402-restricted EBV peptides are as follows: TYPVLEEMF ($BRLF\text{-}1_{198-206}$), DYNFVKQLF ($BMLF\text{-}1_{320-328}$), IYVLVMLVL ($LMP2_{222-230}$), RYSIFFDYM ($EBNA3A_{246-254}$) and TYSAGIVQI ($EBNA3B_{217-225}$). The sequences of the HLA-A*0201-restricted EBV peptides are GLCTLVAML ($BMLF\text{-}1_{280-288}$) and YLQQNWWTL ($LMP1_{159-167}$). AFP-specific or hTERT-specific T cells were stained with the phycoerythrin-conjugated HLA-A*2402 peptide ($AFP_{357-365}$)[11] or HLA-A*2402 peptide ($hTERT_{461-469}$)[20]. All tetramers were purchased from MBL.

Single-cell sorting and RT-PCR. Tetramer-positive cells that had been stimulated with IL-2 and phytohemagglutin for 2 d were single-cell–sorted by FACSAria (Becton Dickinson) into MicroAmp reaction tubes (Applied Biosystems) that contained a cell lysis solution composed of 29.2 μg Dynabeads $Oligo(dT)_{25}$ (Invitrogen), 2.9 μl Lysis/Binding Buffer (Invitrogen) and 0.29 pmol of each gene-specific primer. The sequences of the primers were as follows: alpha-RT 5′-AGCAGTGTTTGGCAGCTCTT-3′, beta1-RT 5′-CTGGCAAAAGAAGAATGTGT-3′ and beta2-RT (5′-ACACAGATTGGGAGCAGGTA-3′). The Dynabeads were then transferred into a solution containing 4.0 U SuperScriptIII (Invitrogen), 0.3 U Murine RNase inhibitor (New England BioLabs), 0.5 mM each dNTP, 5 mM DTT, 0.2% Triton X-100 and 1× First-Strand Buffer (Invitrogen). The reverse transcription reaction was performed for 40 min at 50 °C. After the reverse transcription reaction, the Dynabeads were transferred into another solution containing 8 U of terminal deoxynucleotidyl transferase (Roche), 0.5 mM dGTP, 0.4 U murine RNase inhibitor, 4 mM $MgCl_2$, 0.2% Triton X-100, 50 μM K_2HPO_4 and 50 μM KH2PO4, pH 7.0, and were incubated for 40 min at 37 °C to add a poly-dG tail to the 3′ end of the cDNA. The Dynabeads were then transferred into a new PCR tube containing the first PCR reaction mixture. The first PCR was performed using PrimeSTAR HS DNA polymerase (TaKaRa) according to the manufacturer's instructions with the AP-1, alpha-1st, beta1-1st and beta2-1st primers. The PCR cycles for AP-1 (5′-ACAGCAGGTCAGTCAAGCAGTAGCAGCAGTTCGATAACTTCGAATTCTGCAGTCGACGGTACCGCGGGCCCGGGATCCCCCCCCCCCCDN-3′), alpha-1st (5′-AGAGGGAGAAGAGGGGCAAT-3′), beta1-1st (5′-CCATGACGGGTTAGAAGCTC-3′) and beta2-1st (5′-GGATGAAGAATGACCTGGGAT-3′) were as follows: 5 min at 95 °C followed by 30 cycles of 15 s at 95 °C, 5 s at 60 °C and 1 min 30 s at 72 °C.

The resultant PCR mixtures were diluted 100-fold with water, and 2 μl of the diluted PCR mixtures were added to 23 μl of the nested PCR mixture as template DNA. The nested PCR was performed in a reaction mixture similar to that for the first PCR but with the adaptor primer AP-2 (5′-AGCAGTAGCAGCAGTTCGATAA-3′) and a primer specific for the constant region of TCRα (alpha-nest, 5′-GGTGAATAGGCAGACAGACTT-3′) or TCRβ (beta-nest, 5′-GTGGCCAGGCACACCAGTGT-3′). The PCR cycles were as follows: 1 min at 98 °C followed by 35 cycles of 15 s at 98 °C, 5 s at 60 °C and 45 s at 72 °C.

The PCR products were then analyzed with the alpha-nest or beta-nest primer by either direct sequencing or sequencing after subcloning into an expression vector. The TCR repertoire was analyzed with the IMGT/V-Quest tool (http://www.imgt.org/)[21].

Retroviral transfection. The cDNAs encoding the TCRα or TCRβ chain were independently inserted into a pMX vector or pMX-IRES-EGFP vector[22], which was then transfected into PLAT-E cells with FuGENE 6 (Roche). The culture supernatant was collected 72 h after transfection and added to human CD8–TG40 cells together with polybrene (Sigma-Aldrich). EBV-specific tetramer binding was analyzed by flow cytometry. For transduction into human PBLs, the TCRα and TCRβ chains were linked by a viral F2A sequence[23] or a P2A sequence[24], cloned into the pMX-IRES-EGFP vector and transfected into the Phoenix A cells. Transduction efficiency was monitored by the expression of EGFP.

Determination of the antigen specificity of cloned TCRs. The antigen specificity of the cloned TCRαβ pairs was analyzed using the CD69 induction assay, tetramer staining or both. Briefly, TCR-expressing human CD8–TG40 cells were incubated overnight with $HLA\text{-}A24^+$ PBLs in the presence of each of the EBV peptides (BRLF-1, BMLF-1, LMP2, EBNA3A or EBNA3B). After incubation, the cell surface expression of CD69 was analyzed by flow cytometry.

Preparation of PBLs transduced with cloned TCR cDNAs. 5×10^5 PBLs were stimulated *in vitro* with CD3/CD28 Dynabeads (Invitrogen) and 30 IU ml^{-1} recombinant hIL-2 (Peprotech) according to the manufacturer's instructions. On day 2, the stimulated PBLs were washed, and 5×10^5 cells were resuspended in the medium containing 30 IU ml^{-1} recombinant hIL-2. The cells were added to each well in the plates that had been coated with 50 μg ml^{-1} retronectin (TaKaRa) and spin-loaded with TCR-encoding retroviral supernatant by centrifuging for 2 h at 1,900*g* at 32 °C. The cells were spun down at 1,000*g* at 32 °C for 10 min and incubated overnight at 37 °C in 5% CO_2. On day 3, the PBLs were transferred onto newly prepared retroviral-coated plates

as on day 2 and cultured with 30 IU ml^{-1} recombinant hIL-2. On day 10, the TCR cDNA–transduced PBLs were evaluated for expression of the appropriate TCR by tetramer staining and flow cytometry.

Cytotoxic T lymphocyte assay. In the case of the AFP-specific and hTERT-specific TCRs, the cytotoxicity of the TCR cDNA–transduced PBLs was measured by the ^{51}chromium release assay[11]. In the case of the EBV-specific TCR, the cytotoxicity of the TCR cDNA–transduced PBLs was measured using the calcein-AM (Wako Pure Chemical) release assay. Briefly, peptide-loaded T2-A24 target cells were labeled with 25 μM calcein-AM for 30 min at 37 °C. Then, the target cells and TCR cDNA–transduced PBLs (effector cells) were plated in 96-well plates at the indicated effector-to-target (E/T) ratios and incubated for 4 h. After incubation, the fluorescence of calcein in the supernatants was measured using FLUOstar OPTIMA microplate reader (BMG LABTECH). The percentage of cytotoxicity was calculated using the following formula: % lysis = (F experiment − F spontaneous)/(F maximal − F spontaneous) × 100.

IFN-γ secretion assay. IFN-γ–secreting cells were detected using the IFN-γ secretion assay (Miltenyi Biotec) according to the manufacturer's instructions. Briefly, PBLs were stimulated with the BRLF-1 peptide for 14 d. After *in vitro* stimulation, the PBLs were stimulated with CD28-specific antibody with or without the BRLF-1-peptide for 6 h. The PBLs were washed and stained with IFN-γ Catch Reagent (Miltenyi Biotec). The PBLs were then suspended in 1 ml medium and incubated for 45 min to allow cytokine secretion. After washing, the PBLs were stained with phycoerythrin-conjugated IFN-γ Detection Reagent (Miltenyi Biotec) and FITC-conjugated CD8-specific antibody.

ELISA assay. ELISA assays were performed according to the manufacturer's instructions. Briefly, 1×10^5 TCR cDNA–transduced PBLs were cocultured with 1×10^5 T2-A24 cells pulsed with specific peptide. After 16 h incubation, the supernatants were collected, and IFN-γ, IL-2 and TNF-α in the supernatant were measured by ELISA (R&D systems). The results shown are the mean ± s.d. of triplicate experiments.

TG40-based TCR downregulation assay. The IC_{50} of the peptide responses of the TCRαβ cDNA–transduced TG40 was determined with TCR downregulation assay[7]. Briefly, human CD8-TG40 cells expressing TCRs specific for BRLF-1 were incubated overnight with T2-A24 cells in the presence of various concentrations of BRLF-1 peptide. After incubation, the CD3ε expression was analyzed by flow cytometry. The percentage of CD3ε expression was calculated using the following formula: % CD3ε expression = (CD3ε expression in the presence of indicated concentration of specific peptide)/(CD3ε expression in the absence of specific peptide) × 100. The IC_{50} values were calculated by probit analysis[25].

ELISPOT assay. IFN-γ ELISPOT assays were performed as previously reported[26]. 96-well multiscreen filter plates (Millipore) were coated with 5 μg ml^{-1} human IFN-γ–specific antibody (catalog number DY285, R&D Systems) and blocked with culture medium. Then, EBV-transformed JTL-LCL cells with or without HLA-ABC–specific antibody (clone B9.12.1) (Beckman Coulter) were plated with TCR cDNA–transduced PBLs at the indicated cell numbers and incubated for the indicated times. After incubation, 1 μg ml^{-1} biotin-conjugated human IFN-γ–specific antibody (catalog number BAF285, R&D systems) was added, followed by alkaline phosphatase–conjugated streptavidin (Sigma). After washing, a mixture of 3-bromo-4-chloro-3-indolyl-phosphate toluidine and *p*-nitroblue tetrazolium chloride (Sigma) was added to detect the immunospots.

17. Ueno, T., Tomiyama, H., Fujiwara, M., Oka, S. & Takiguchi, M. Functionally impaired HIV-specific CD8 T cells show high affinity TCR-ligand interactions. *J. Immunol.* **173**, 5451–5457 (2004).
18. Morita, S., Kojima, T. & Kitamura, T. Plat-E: an efficient and stable system for transient packaging of retroviruses. *Gene Ther.* **7**, 1063–1066 (2000).
19. Kinsella, T.M. & Nolan, G.P. Episomal vectors rapidly and stably produce high-titer recombinant retrovirus. *Hum. Gene Ther.* **7**, 1405–1413 (1996).
20. Mizukoshi, E. *et al.* Cytotoxic T cell responses to human telomerase reverse transcriptase in patients with hepatocellular carcinoma. *Hepatology* **43**, 1284–1294 (2006).
21. Giudicelli, V., Chaume, D. & Lefranc, M.P. IMGT/V-QUEST, an integrated software program for immunoglobulin and T cell receptor V-J and V-D-J rearrangement analysis. *Nucleic Acids Res.* **32**, W435–W440 (2004).
22. Onishi, M. *et al.* Applications of retrovirus-mediated expression cloning. *Exp. Hematol.* **24**, 324–329 (1996).
23. Ryan, M.D., King, A.M. & Thomas, G.P. Cleavage of foot-and-mouth disease virus polyprotein is mediated by residues located within a 19 amino acid sequence. *J. Gen. Virol.* **72**, 2727–2732 (1991).
24. Leisegang, M. *et al.* Enhanced functionality of T cell receptor-redirected T cells is defined by the transgene cassette. *J. Mol. Med. (Berl)* **86**, 573–583 (2008).
25. Goldstein, A. *Biostatistics: An Introductory Text* (Macmillan, New York, 1964).
26. Jin, A. *et al.* A rapid and efficient single-cell manipulation method for screening antigen-specific antibody-secreting cells from human peripheral blood. *Nat. Med.* **15**, 1088–1092 (2009).

DOI: 10.1002/eji.201343531 Eur. J. Immunol. 2013. 43: 2956–2968

European Journal of Immunology

Adipose tissue derived stromal stem cell therapy in murine ConA-derived hepatitis is dependent on myeloid-lineage and CD4$^+$ T-cell suppression

Mami Higashimoto[*1], *Yoshio Sakai*[*2,3], *Masayuki Takamura*[1], *Soichiro Usui*[1], *Alessandro Nasti*[1], *Keiko Yoshida*[1], *Akihiro Seki*[1], *Takuya Komura*[1], *Masao Honda*[3], *Takashi Wada*[2], *Kengo Furuichi*[4], *Takahiro Ochiya*[5] *and Shuichi Kaneko*[1,3]

[1] Disease Control and Homeostasis, Kanazawa University, Kanazawa, Japan
[2] Department of Laboratory Medicine, Kanazawa University, Kanazawa, Japan
[3] Department of Gastroenterology, Kanazawa University Hospital, Kanazawa, Japan
[4] Division of Blood Purification, Kanazawa University Hospital, Kanazawa, Japan
[5] Division of Molecular and Cellular Medicine, National Cancer Center Research Institute, Tokyo, Japan

Mesenchymal stromal stem cells (MSCs) are an attractive therapeutic model for regenerative medicine due to their pluripotency. MSCs are used as a treatment for several inflammatory diseases, including hepatitis. However, the detailed immunopathological impact of MSC treatment on liver disease, particularly for adipose tissue derived stromal stem cells (ADSCs), has not been described. Here, we investigated the immunomodulatory effect of ADSCs on hepatitis using an acute ConA C57BL/6 murine hepatitis model. i.v. administration of ADSCs simultaneously or 3 h post injection prevented and treated ConA-induced hepatitis. Immunohistochemical analysis revealed higher numbers of CD11b$^+$, Gr-1$^+$, and F4/80$^+$ cells in the liver of ConA-induced hepatitis mice was ameliorated after the administration of ADSCs. Hepatic expression of genes affected by ADSC administration indicated tissue regeneration-related biological processes, affecting myeloid-lineage immune-mediating Gr-1$^+$ and CD11b$^+$ cells. Pathway analysis of the genes expressed in ADSC-treated hepatic inflammatory cells revealed the possible involvement of T cells and macrophages. TNF-α and IFN-γ expression was downregulated in hepatic CD4$^+$ T cells isolated from hepatitis livers co-cultured with ADSCs. Thus, the immunosuppressive effect of ADSCs in a C57BL/6 murine ConA hepatitis model was dependent primarily on the suppression of myeloid-lineage cells and, in part, of CD4$^+$ T cells.

Keywords: Adipose tissue derived stromal stem cells · Anti-inflammatory effects · CD4$^+$ T cells · ConA hepatitis · Myeloid-lineage cells

Additional supporting information may be found in the online version of this article at the publisher's web-site

Correspondence: Dr. Shuichi Kaneko
e-mail: skaneko@m-kanazwa.jp

*These authors contributed equally to this work.

Introduction

Mesenchymal stromal stem cells (MSCs) are somatic cells that reside in the mesenchymal tissues, such as the BM, umbilical cord, and adipose tissue [1,2]. MSCs are able to differentiate into several types of cells (pluripotent) in the same lineage, such as chondrocytes, osteocytes, adipocytes, and cardiomyocytes, as well as those of different lineages, such as hepatocytes. Because of this differentiation capability, they have been studied as a possible application in regenerative therapy of miscellaneous impaired organs, such as breast reconstruction [3] and repair of ischemic heart tissue [4]. Another intriguing characteristic of MSCs is their immunomodulatory potency [5]. Because most liver diseases, including viral hepatitis [6,7], primary biliary cirrhosis [8], autoimmune hepatitis [9], and steatohepatitis [10], are associated with hepatic inflammatory cells [11], elucidation of the effect of MSCs on hepatic inflammation is important when considering the use of MSCs for treating liver diseases. Although the efficacy of MSC treatment of liver diseases has been reported [12], the detailed immunopathological impact of MSC treatment on liver diseases, particularly for adipose tissue derived stromal stem cells (ADSCs), has not been investigated.

ConA, a plant lectin [13], is frequently used to induce acute hepatitis in rodents [14] to model the pathological features of autoimmune hepatitis. Although this model is mediated mainly by lymphocyte-lineage cells such as T cells and NKT cells, Kupffer cells/macrophages also participate in hepatitis. Therefore, evaluating the therapeutic efficacy of ADSCs in this murine hepatitis model is important. Although the potential efficacy of ADSCs in a BALB/c ConA hepatitis model has been reported [15], the immunopathology has not been investigated.

We confirmed that immediate i.v. administration of ADSCs after ConA injection prevented hepatitis. We also observed that administering ADSCs 3 h after the ConA injection resulted in successful treatment of hepatitis, as the liver was already infiltrated by $CD11b^+$ and $Gr\text{-}1^+$ inflammatory cells. Gene expression analysis of the liver showed that ADSC treatment affected myeloid-lineage cells, providing repair and regenerative effects in ConA-induced hepatitis mice. Moreover, gene expression analysis of hepatic inflammatory cells indicated pathways related to T cells and monocyte-lineage cells. Pathologically important cytokines such as TNF-α and IFN-γ were upregulated in $CD4^+$ T cells isolated from ConA-induced hepatitis mice but were significantly suppressed by co-culture with ADSCs. Thus, the anti-inflammatory effects of ADSCs in the C57BL/6 murine ConA hepatitis model were mediated by the suppression of myeloid-lineage and $CD4^+$ T cells.

Results

Characteristics of the immune response in ConA-induced hepatitis mice

To examine the characteristics of ConA-induced acute hepatitis, we injected 300 μg ConA into C57BL/6 female mice ($n = 4$) and determined serum alanine transferase (ALT) and lactate dehydrogenase (LDH) activities. Serum ALT and LDH activities were elevated through 24 h (Fig. 1A). The macroscopic appearance and histology of the liver obtained 24 h after ConA injection revealed intense necrosis (Fig. 1B). The immunohistochemical analysis showed that the number of $CD4^+$ T cells in the liver peaked at 6 h after the ConA injection, and remained high for 24 h (Fig. 1C and D). The numbers of $CD11b^+$ cells and $Gr\text{-}1^+$ cells accumulated in the liver increased at 3 h and reached a maximum at 12 h after ConA injection (Fig. 1C and D). The numbers of $F4/80^+$ monocyte/macrophage lineage cells increased at 6 h after the ConA injection, but returned to basal levels after 24 h (Fig. 1C and D). We also assessed the frequency of $CD11b^+/Gr\text{-}1^+$ cells, as a phenotype of myeloid-derived suppressor cells (MDSCs), in ConA hepatitis mice at 6 h ($n = 3$). The frequency of $CD11b^+/Gr\text{-}1^+$ cells was higher than that in WT mice (Fig. 1E). Scavenger receptor CD204 expression was higher in $CD11b^+/Gr\text{-}1^+$ cells than $CD11b^+/Gr\text{-}1^-$ cells (Fig. 1F), and the population gated for $CD11b^+$ cells contained granulocytic $Ly\text{-}6C^+/Ly\text{-}6G^+$ cells as well as monocytic $Ly\text{-}6C^+/Ly\text{-}6G^-$ cells (Fig. 1G).

To determine the type of immune-mediating cells involved in ConA-induced acute hepatitis, we depleted mice of various immune cell subpopulations ($n = 4$ per group). Mice that were pretreated with clodronate, a reagent that depletes monocyte-macrophage lineage cells [16], followed by injection of ConA, did not show a significant elevation in serum ALT or LDH activity (Fig. 1H). Mild elevation of serum activity for these enzymes in mice depleted of $CD4^+$ T cells was observed, whereas depletion of $CD8^+$ T cells had no significant effect. These results suggest the importance of monocyte-macrophage myeloid-lineage cells, as well as the contribution of $CD4^+$ T cells, in ConA-induced hepatitis.

ConA-induced acute hepatitis is ameliorated by i.v. administration of ADSCs in vivo

Next, we determined the therapeutic efficacy of ADSCs in the ConA-induced hepatitis model. We obtained and expanded stromal cells from adipose tissue by passaging them eight to ten times (Fig. 2A). Almost all cells expressed the mesenchymal lineage markers, CD29 and CD44 (Fig. 2B). With regard to stem cell markers [17], approximately 40% and 73% of cells expressed CD105 and CD90, respectively (Fig. 2B). Moreover, the cells were pluripotent and were able to differentiate into osteocytes, chondrocytes, and adipocytes (Fig. 2C–F). When 1×10^5 ADSCs were administered via the tail vein immediately after ConA injection in mice ($n = 3$), the elevation of serum ALT and LDH activity was substantially ameliorated, compared with mice without ADSC treatment ($n = 4$) 24 h after injection (Fig. 3A). In terms of therapeutic efficacy, 1×10^5 ADSCs were administered to mice 3 h after ConA injection ($n = 3$), serum ALT and LDH activities were significantly reduced in acute hepatitis mice treated with ADSCs, compared with ConA-induced hepatitis mice without treatment ($n = 4$), 24 h after ConA administration (Fig. 3B). The macroscopic